Vol. 10 • No. 3 • February 9 • 2026

www.small-methods.com

small methods

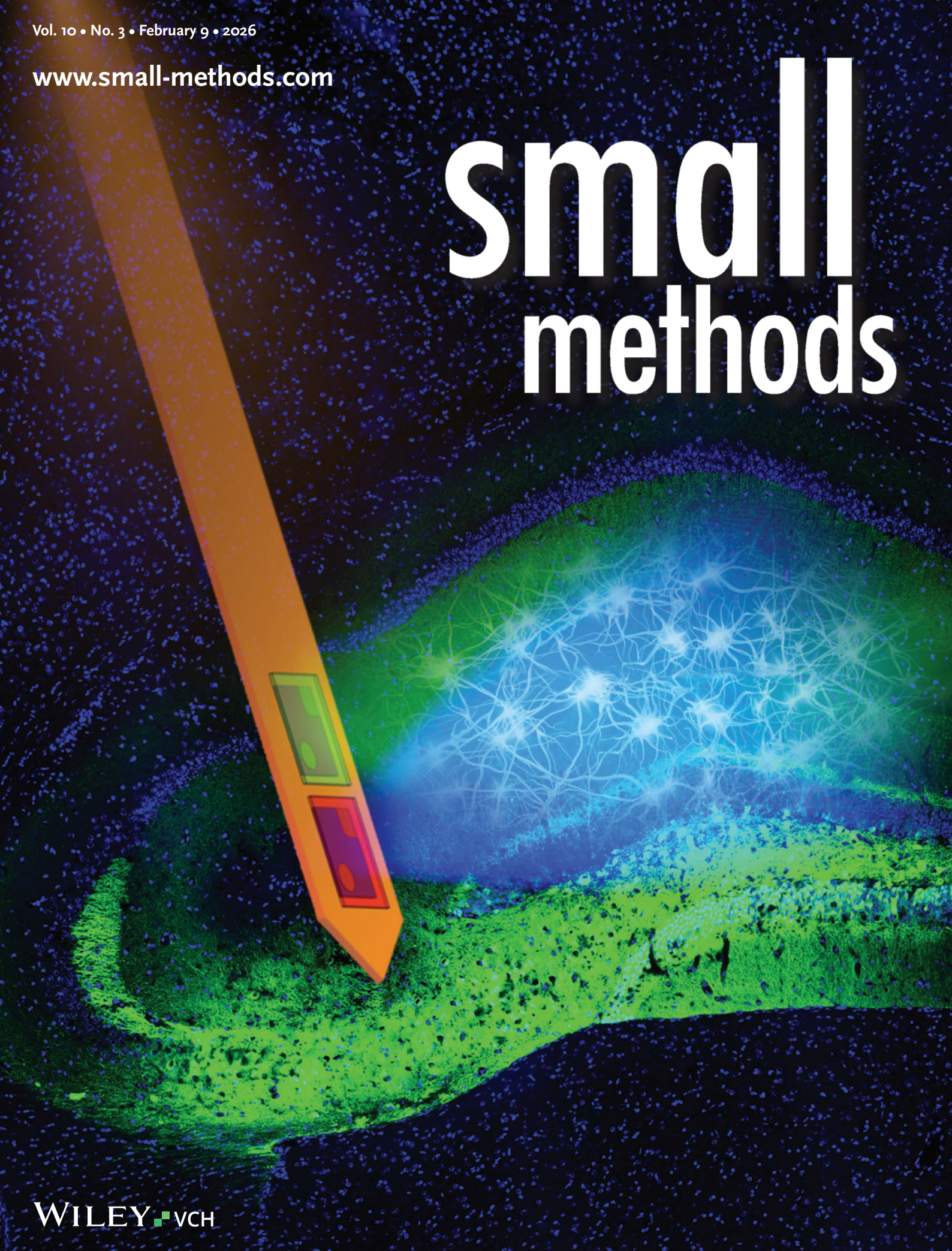

WILEY VCH

RESEARCH ARTICLE

small methods
www.small-methods.com

A Wireless Photometric Probe to Capture Calcium Activities During Hippocampal Seizures in Freely Moving Mice

Wenxin Zhao, Jiazheng Chen, Lizhu Li, Xinli Song, Wanghan Zhang, Guo Tang, Haijian Zhang, Xue Cai, Dawid Sheng, Yu Zhao, Xinyue Wang, Kun Li, Lan Yin, He Ding, Xiaochuan Dai, Changbo Liu, and Xing Sheng**

Exploring the coding mechanisms of the nervous system and their associated functions holds great value in neuroscience research. Specifically, monitoring deep-brain neuronal activities with high specificity and minimal invasiveness is crucial. In this study, the development and application of a wireless photometric probe system is presented to monitor calcium (Ca^{2+}) dynamics in the hippocampus during seizure events in freely moving mice. The probe integrates thin-film, microscale optoelectronic devices, including a micro light-emitting diode (micro-LED) and a photo detector, to excite and capture fluorescent emissions of the genetically encoded Ca^{2+} indicator (GCaMP). Wavelength-selective optical designs minimize the spectral crosstalk and optimize the detection of green fluorescence signals. Additionally, a portable, miniaturized wireless circuit module powers the devices and remotely transmits data. In vitro experiments validate the probe's capability to detect fluorescence signals in both ambient and aqueous environments, while in vivo experiments reveal its efficacy in capturing Ca^{2+} dynamics during seizure occurrences provoked by electrical stimulations as well as drug administrations in the hippocampus of behaving mice. The wireless photometric probe system developed here offers a promising tool for neuroscience research, particularly in studying complex behaviors and disease models in freely moving animals.

1. Introduction

The study of brain perception and regulation has long been a focus of neuroscience research. To achieve this goal, understanding the information coding rules and modulation mechanisms of the nervous system is essential.[1–5] Over the years, various recording tools, such as microelectrode arrays,[6–9] chemical sensors,[10–13] and magnetic resonance imaging,[14–18] have been developed to monitor neuronal activities. These approaches primarily capture single-cell electrophysiology or the collective activity of neuron groups within a certain spatial range. To link specific neuronal activity to behaviors or processes, genetically encoded fluorescence indicators and optical recording methods have been developed for cell-specific monitoring of neuronal activities.[19–25] Through genetic engineering, fluorescent indicator proteins can be expressed in

W. Zhao, J. Chen, W. Zhang, G. Tang, X. Cai, D. Sheng, Y. Zhao, X. Sheng
Department of Electronic Engineering
Beijing National Research Center for Information Science and Technology
Institute for Precision Medicine
State Key Laboratory of Flexible Electronics Technology
IDG/McGovern Institute for Brain Research
Tsinghua University
Beijing 100084, China
E-mail: xingsheng@tsinghua.edu.cn

L. Li
School of Life Science and Technology
University of Electronic Science and Technology of China
Sichuan 611731, China

X. Song, K. Li
School of Life Sciences
Tsinghua-Peking Joint Center for Life Sciences
IDG/McGovern Institute for Brain Research at Tsinghua
Tsinghua University
Beijing 100084, China

C. Liu
School of Materials Science and Engineering
Beihang University
Beijing 100191, China
E-mail: liuchb@buaa.edu.cn

C. Liu
Key Laboratory of Intelligent Sensing Materials and Chip Integration Technology of Zhejiang Province
Hangzhou Innovation Institute of Beihang University
Hangzhou 310051, China

L. Yin
School of Materials Science and Engineering
State Key Laboratory of Flexible Electronics Technology
Key Laboratory of Advanced Materials of Ministry of Education
Tsinghua University
Beijing 100084, China

The ORCID identification number(s) for the author(s) of this article can be found under https://doi.org/10.1002/smtd.202500470

DOI: 10.1002/smtd.202500470

specific neuron populations, being the fluorescent labels after bonding to the target ions or molecules,[26–31] and this provides a cytological foundation for fluorescence recordings. In particular, calcium (Ca^{2+}) dynamics is one of the most widely used fluorescence recording modalities to monitor neural activities, based on monitoring the change of Ca^{2+} concentration within cells or Ca^{2+} flow across cell membranes[32–35] through the variation of fluorescence intensity.[36–42]

In synergy with genetically encoded Ca^{2+} indicators, various types of fluorescence microscopes have been extensively explored to record Ca^{2+} dynamics for cultured cells, acute brain slices, and living animals,[43–45] while fiber-based photometric systems enable the detection of Ca^{2+} signals in the deep brain.[46–48] These conventional systems rely on tethered instruments, which may influence animal behaviors and pose constraints in studying complex social interactions. More recently, researchers have developed wirelessly operated photometric probes for monitoring Ca^{2+} fluorescence in freely moving animals and eliminated the limitations of wired devices.[49,50] Based on microscale optoelectronic devices, these miniaturized probes reduce tissue damage and successfully monitor the Ca^{2+} dynamics in the deep brain of mice. Nevertheless, such device systems still hold potential for further optimization and in-depth explorations in multiple aspects: i) State-of-the-art probes are still based on flip-chip bonded light-emitting diodes (LEDs) and/or photo detectors with thicknesses of tens of micrometers. Thin-film devices can be implemented to mitigate the tissue lesion after implantation; ii) Additional optical designs can be introduced to further minimize the spectral crosstalk and improve the fluorescence signal quality; iii) Current infrared LED based data transponders possess limited communication distance (< 1 m) and data transmission rate (≈50 kbps); iv) More sophisticated animal behavioral paradigms and disease models can be investigated with these wireless photometric systems.

In this paper, we develop a wireless photometric probe system to monitor Ca^{2+} activities in a mouse seizure model. The implantable probe integrates thin-film, microscale optoelectronic devices (a micro-LED and a photo detector) to excite and capture fluorescence signals of a genetically encoded Ca^{2+} fluorescence protein (GCaMP). Both the LED and the detector implement spectral selective filter designs to optimize the signal-to-noise ratio. A portable, miniaturized circuit supplies power to the probe, processes and transmits data via a Bluetooth transponder. We conduct in vitro experiments to evaluate the fluorescence detection capability of the system. Furthermore, we implant these wireless probes into the hippocampus of mice, capture and quantitatively compare real-time Ca^{2+} dynamics during seizure events induced by electrical or chemical stimuli. With these results, we anticipate that such a wireless photometric system will find broad applications in neuroscience research.

X. Wang, X. Dai
School of Biomedical Engineering
Tsinghua University
Beijing 100084, China
H. Zhang, H. Ding
Beijing Engineering Research Center of Mixed Reality and Advanced Display
School of Optics and Photonics
Beijing Institute of Technology
Beijing 100081, China

2. Results

2.1. Design, Fabrication, and Optoelectronic Performance of the Photometric Probe

Figure 1a shows a schematic diagram (left) and an exploded view (right) of the photometric probe for recording Ca^{2+} fluorescence in the brain, while Figure 1b presents optical images of a probe. The key functional optoelectronic components on the probe include an indium gallium nitride (InGaN) blue micro-LED for optically exciting the genetically encoded Ca^{2+} indicator (GCaMP) and an indium gallium phosphide (InGaP) photodiode to record the green fluorescence emission from GCaMP. The fluorescence signal of GCaMP is Ca^{2+}-specific and selective, and not sensitive to other signals like blood flow and oxygenation. Tables S1 and S2 (Supporting Information) provide detailed epitaxial structures of the InGaN blue LED and the InGaP detector originally grown on single-crystalline sapphire and gallium arsenide (GaAs) substrates, respectively. Compared to previously reported photometric probe involving detectors made of GaAs,[49] the InGaP detector we use here has two advantages: i) The InGaP diode has a bandgap of ≈1.9 eV, which is large than that of silicon (Si) (≈1.1 eV) and GaAs (≈1.4 eV), so it has a smaller dark current than GaAs detectors with a similar size; ii) Compared to the GaAs detector, the InGaP detector only has a 100 nm thick GaAs contact layer, so it contains less arsenide (As) element and has less toxicity. Through photolithographic patterning, epitaxial liftoff and transfer printing,[51–53] fully formed freestanding, thin-film InGaN micro-LEDs and InGaP detectors (lateral dimensions of 125 × 180 μm^2 and overall thicknesses of 7.3 and 2.8 μm, respectively) are integrated onto flexible polyimide (PI) based probe substrates.

Figure 1c shows the current–voltage (*I*–*V*) characteristic curve and an image (inset) of an illuminating blue micro-LED. Although the emission spectrum of this micro-LED is chosen to reasonably overlap with the excitation of GCaMP (Figure 1e), its long-wavelength tail extending to the green range (>500 nm) will mix with the GCaMP emission spectrum and cannot be distinguished by the detector. Therefore, here we design and fabricate a thin-film short-pass filter (SP495) and transfer it onto the micro-LED.[54] Figure 1d plots the measured transmission spectrum of the SP495 filter, which presents a sharp cutoff at 495 nm. Such a filter design markedly removes the green part of the LED emission above 495 nm, while the remaining LED emission is still capable of exciting GCaMP (Figure 1e). Within the tissue, this spectral portion below 495 nm mixes with the green fluorescence of GCaMP and should be further blocked before entering the detector. Therefore, the detector is coated with a band-selective filter (ABS473),[49,55] which has strong absorbance around 473 nm and greatly minimizes the interference of the LED emission (Figure 1f). With the ABS473 filter, the InGaP detector exhibits prominently reduced external quantum efficiency (EQE) around 473 nm (emission from the blue LED), while maintaining high response from 500 to 600 nm that covers the fluorescence emission of GCaMP (Figure 1g; Figure S1, Supporting Information). Figure 1h shows *I*–*V* curves of a coated detector

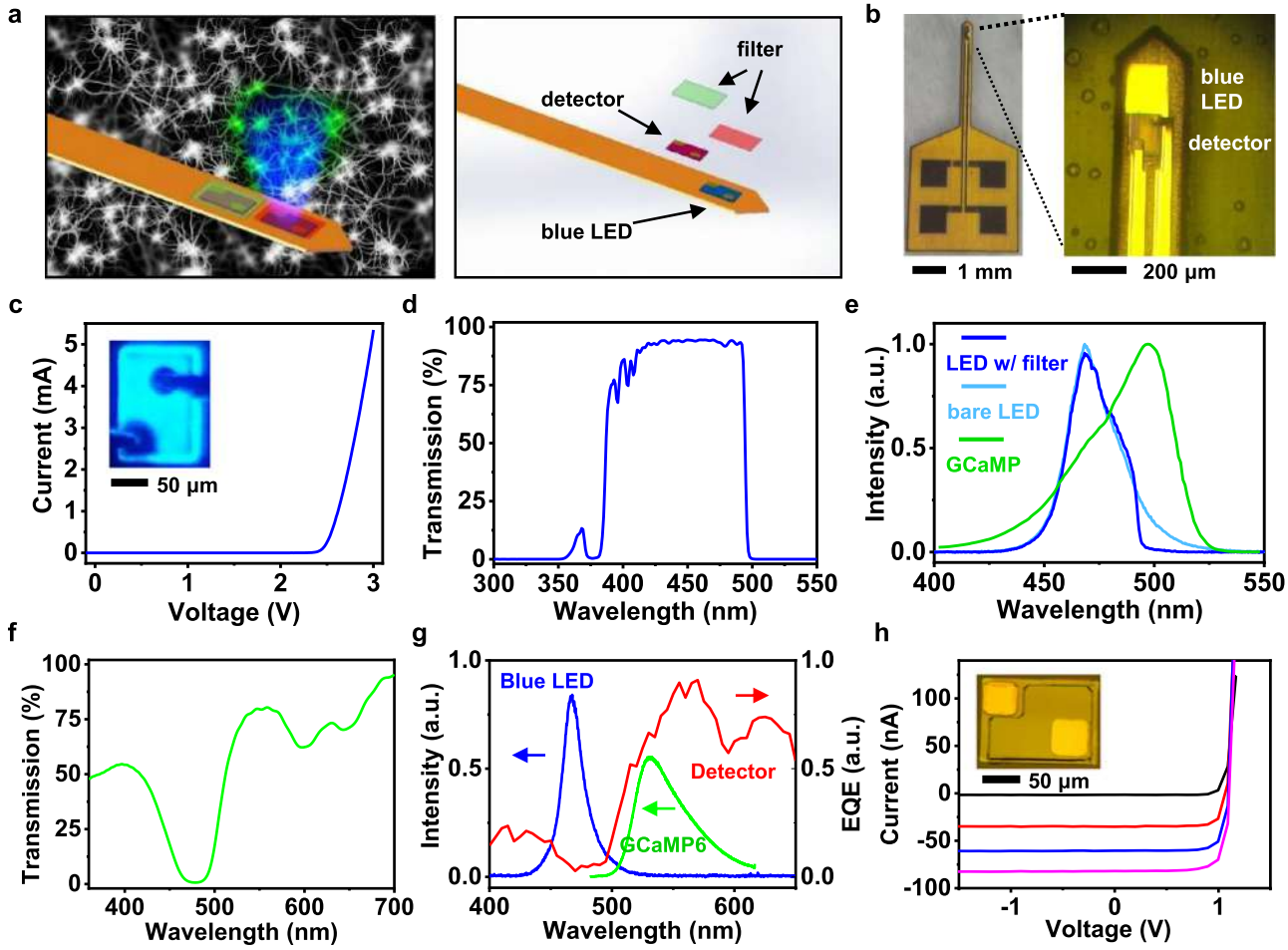

Figure 1. Schemes, images, and properties of the implantable photometric probe for calcium (Ca^{2+}) fluorescence detection, as well as thin-film microscale optoelectrical devices. a) Schematic diagram (left) and exploded view (right) of the photometric probe operating in the brain. The probe structure incorporates an InGaN blue LED with a short-pass filter, an InGaP photo detector with a blue-absorbing dye filter, both of which are transferred to a PI substrate. b) Top-view photographs of a probe. c) Current–voltage (*I–V*) characteristic curve and microscopic image (inset) of the blue LED. d) Transmission spectrum of the short-pass filter (SP495) applied to the LED. e) Emission spectra of the LED with (dark blue) and without (light blue) the short-pass filter, along with the excitation spectrum of GCaMP (green dashed line). f) Transmission spectrum of the dye filter (ABS473). g) External quantum efficiency (EQE) spectrum of the detector with the dye filter, along with the emission spectra of the blue LED and GCaMP6. h) *I–V* curves of the detector under illumination at 530 nm (power density 0, 1.6, 2.9, and 4.0 mW cm^{-2}, from top to bottom).

responding to various illumination intensities (from 0 to 4.0 mW cm^{-2}) at 530 nm. We observe that the detector has an open-circuit voltage of ≈1.0 V, and its photogenerated current is linearly related to the light power, which can be exploited for green fluorescence detection.

2.2. In Vitro Performance of the Photometric System

We establish a circuit module to wirelessly control the implantable photometric probe, and **Figure** 2a presents the designed circuit block diagram. The wireless system consists of two main components: an implantable probe to excite and detect Ca^{2+} fluorescence in the brain, and an extracranial battery-powered Bluetooth module for wireless transmission. Compared to previously reported photometric probe based on IR data transmission,[49,50] Bluetooth communication is more advantageous in multiple aspects: i) Its extended operational range enables greater freedom of animal movement while maintaining robust connection stability; ii) The theoretical maximum data rate of 2 Mbps (with practical throughput typically of ≈100 kbps)[56] effectively meets the high sampling requirements imposed by advanced fluorescent indicators (e.g., jGCaMP8f, $\tau = 6.6 \pm 1.0$ ms[57]) during complex neural activity studies, high-resolution recordings, or multi-subject experiments (requiring ≈70 kbps throughput if monitoring 3 objects with 16-bit resolution and 10 samples per characteristic peak); iii) Bluetooth Low Energy (BLE) mode ensures prolonged operational duration. To optimize wireless performance, a ceramic antenna is integrated into the printed circuit board (PCB). The implemented wireless module achieves a stable connection at a distance up to 5 m with a sustained data throughput of 6 kbps, fulfilling our requirements for data acquisition. Figure 2b shows a photograph of a

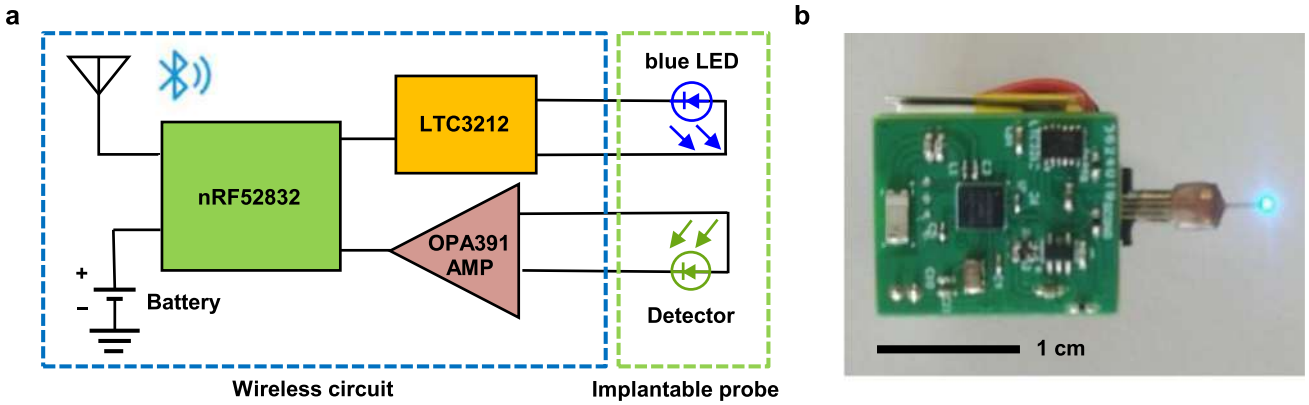

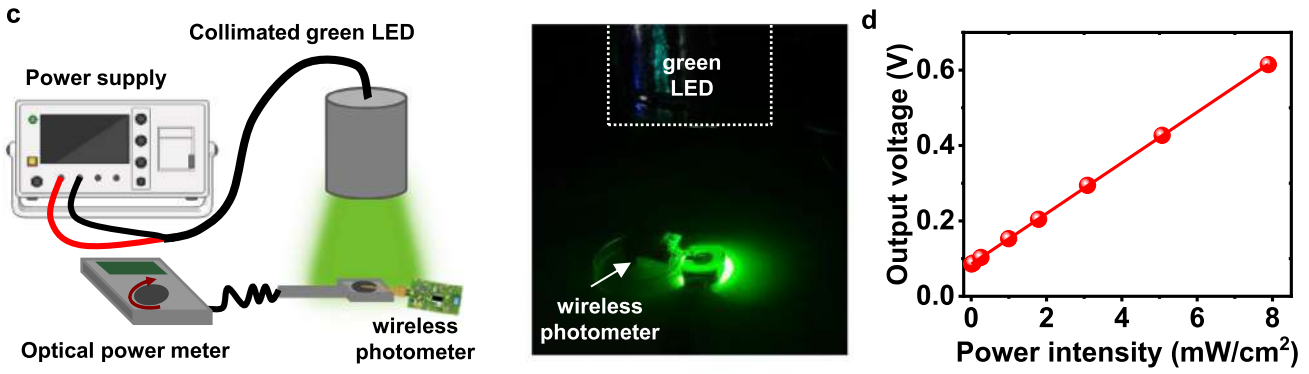

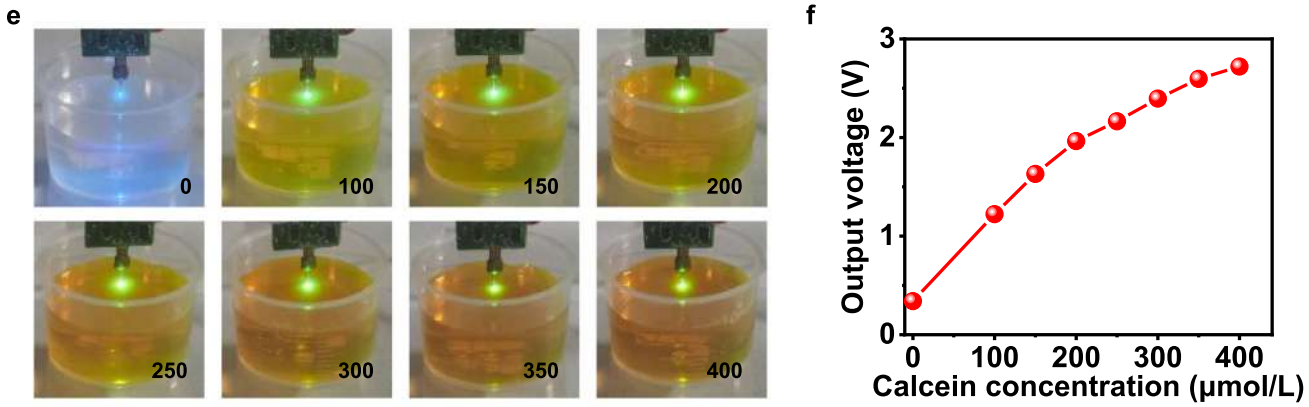

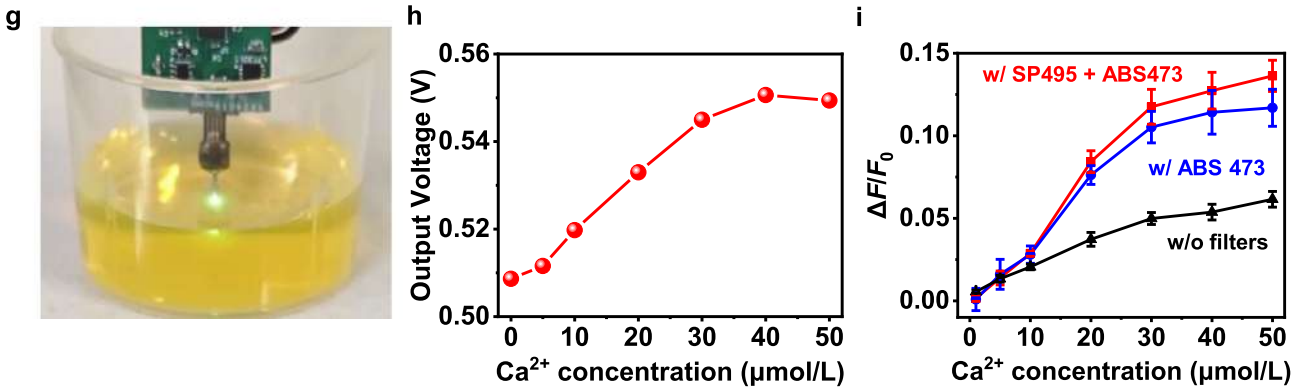

probe powered by a wireless circuit. The schematic diagram of the wireless control module and the layout of the designed PCB are shown in Figures S2 and S3 (Supporting Information). The PCB has a mass of 1.1 g and dimensions of 17.5 × 14.3 mm^2. The lithium (Li) battery weighs 1.3 g with a charge capacity of 60 mAh and provides continuous operation for at least 6 h.

We conduct in vitro experiments in ambient and aqueous environments to evaluate the detection capability of the wireless photometric system. Shown in Figure 2c, a collimated beam generated from a power-tunable green LED is incident on a photometric probe, and its intensity is simultaneously measured by a commercial optical power meter. The detector on the probe captures the photons and generates photocurrents, which are amplified and converted into photo-voltage signals by the circuit module. Figure 2d shows that the measured photo voltage and the incident light intensity exhibit a linear relationship. We then assess the probe performance in an aqueous calcium chloride ($CaCl_2$) (500 µmol L^{-1}) solution containing calcein with different concentrations (0–400 µmol L^{-1}) (Figure 2e). When Ca^{2+} is present in the solution, calcein exhibits strong green fluorescence when excited by the blue LED, and its excitation and emission spectra are similar to those of GCaMP.[36,58] Figure 2f shows the photo voltage measured from the wireless probe as a function of the calcein concentration. The output signal is linearly proportional to the calcein concentration at a low level (<200 µmol L^{-1}) and gradually saturates at an increased calcein level. We further evaluate the system's detection capability by adjusting Ca^{2+} concentrations (from 0 to 50 µmol L^{-1}) in a calcein solution (50 µmol L^{-1}, pH 13) (Figure 2g). As the Ca^{2+} level increases, the output signal increases, presents a saturation trend at ≈50 µmol L^{-1} (Figure 2h). We also compare photo responses for probes with different filter configurations (Figure 2i). Among different designs, the probe with both SP495 and ABS473 filters manifests the highest fluorescence response ($\Delta F/F_0$), validating the efficacy of the filter design.

2.3. In Vivo Experiments of the Photometric System

We implant the wireless photometric probe into the deep brain of mice and assess its fluorescence detection capability in vivo (**Figure 3a**). Comparison of motion trajectory for mice with and without the wireless module (Figure S4, Supporting Information) shows that the system does not interfere with the animal's locomotive behavior. A photometric probe is inserted in the mouse hippocampus along with a tungsten wire-based stimulation electrode,[53] with the 3D scheme presented in Figure 3b. The stimulation electrode generates biphasic pulses (current 0.4 mA, pulse width 1 ms, duty cycle 50%, frequency 60 Hz, duration 1 s) in the CA1 region to provoke seizure activities, while the photometric probe can be inserted into the ipsilateral or contralateral CA3 region for Ca^{2+} detection. Approximately one month prior to the probe implantation, adeno-associated viruses (AAVs) carrying Ca^{2+} fluorescent protein-related (jGCaMP7b) genes are injected into CA3 (Figure 3c). Figure 3d presents a fluorescence image of the brain slice showing the expression of jGCaMP7b and the probe trajectory 4 days post-probe implantation. Figure 3e illustrates the schematic diagram of wireless Ca^{2+} fluorescence recording in mice with kindling (electrical stimulation) induced seizure. Connected to a freely moving mouse, a pulse generator (TECHMAN BL-420S) stimulates CA1 by kindling and provokes epileptic activities, while the wireless photometric system dynamically records and transmits Ca^{2+} fluorescence data to a computer during seizure events. Figure S5 (Supporting Information) shows the immunohistochemistry results (GFAP and Iba1) of mouse brain slices on day 1 and day 21 after the probe implantation. The recorded lesion areas have a size of ≈200 µm (similar to the probe width), indicating that the probe produces minimal inflammation response and no noticeable displacement after chronic implantation.

2.4. In Vivo Ca^{2+} Recording During Seizure Activities

We apply the photometric probe to capture in vivo Ca^{2+} dynamics during hippocampal seizures in mice. In clinical practice, mesial temporal lobe epilepsy is the most common seizure disorder, and its pathological basis is related to the asymmetric pattern of hippocampal neuron loss within the endfolium (hilus and CA3) and CA1.[59] Research indicates that activation of pyramidal neurons in CA1 can reliably induce generalized seizures in non-epileptic mice.[60] In our experiments, the stimulation electrode is implanted into CA1, while the photometric probe is positioned either in the ipsilateral or the contralateral CA3 (**Figure 4a**). Figure 4b presents continuously monitored Ca^{2+} fluorescent signals in the ipsilateral (left) and the contralateral (right) CA3 during sequential kindling over multiple trials. We extract Ca^{2+} signals from two minutes before the first kindling to five minutes after several kindlings, and perform statistical analysis to identify differences and similarities in the collected signals between the two conditions. After each kindling, a strong Ca^{2+} fluorescence spike ($\Delta F/F_0 > 0.2$) always occurs in both the ipsilateral and the contralateral CA3. Figure 4c displays averaged Ca^{2+} spikes responding to kindlings. These strong Ca^{2+} responses are likely to be associated with the enhanced neural activities provoked by kindling.[61–64] We quantitatively compare Ca^{2+} responses upon kindlings in the ipsilateral and the contralateral CA3, in terms of their signal latencies and magnitudes. After kindling, peaks of Ca^{2+} spikes appear at almost the same time (latency 30–60 s) in the ipsilateral and the contralateral CA3 after kindling (Figure 4d). By contrast, peak values for Ca^{2+} spikes

Figure 2. Circuit design and performance of the wireless photometric system. a) Block diagram of the wireless system, comprised of a battery-powered Bluetooth module and an implantable probe. b) Image of a probe powered by a wireless circuit. c) Schematic diagram (left) and photograph (right) showing the experimental setup for testing the system. d) Photo response (output voltage) of the wireless system measured under 530 nm illumination. e) Photos showing fluorescent detection by the probe immersed in aqueous $CaCl_2$ (500 µmol L^{-1}) solutions containing calcein with different concentrations (from 0 to 400 µmol L^{-1}). f) Photo response of the wireless system as a function of the calcein concentration. g) Photo showing fluorescent detection by the probe immersed in the aqueous calcein (50 µmol/L) solution. h) Photo response of the wireless system as a function of the Ca^{2+} concentration (the solution pH is adjusted to 13). i) Relative Ca^{2+} fluorescence intensity change ($\Delta F/F_0$) detected by probes (each line is the result from 3 individual tests in $n = 3$ probes) with the shortpass filter (SP495) on the LED and dye filter (ABS473) on the detector (red curve), with only ABS473 filter (blue curve) and without filters (black curve). The baseline signal (F_0) is the photo signal captured when the Ca^{2+} concentration is 0.

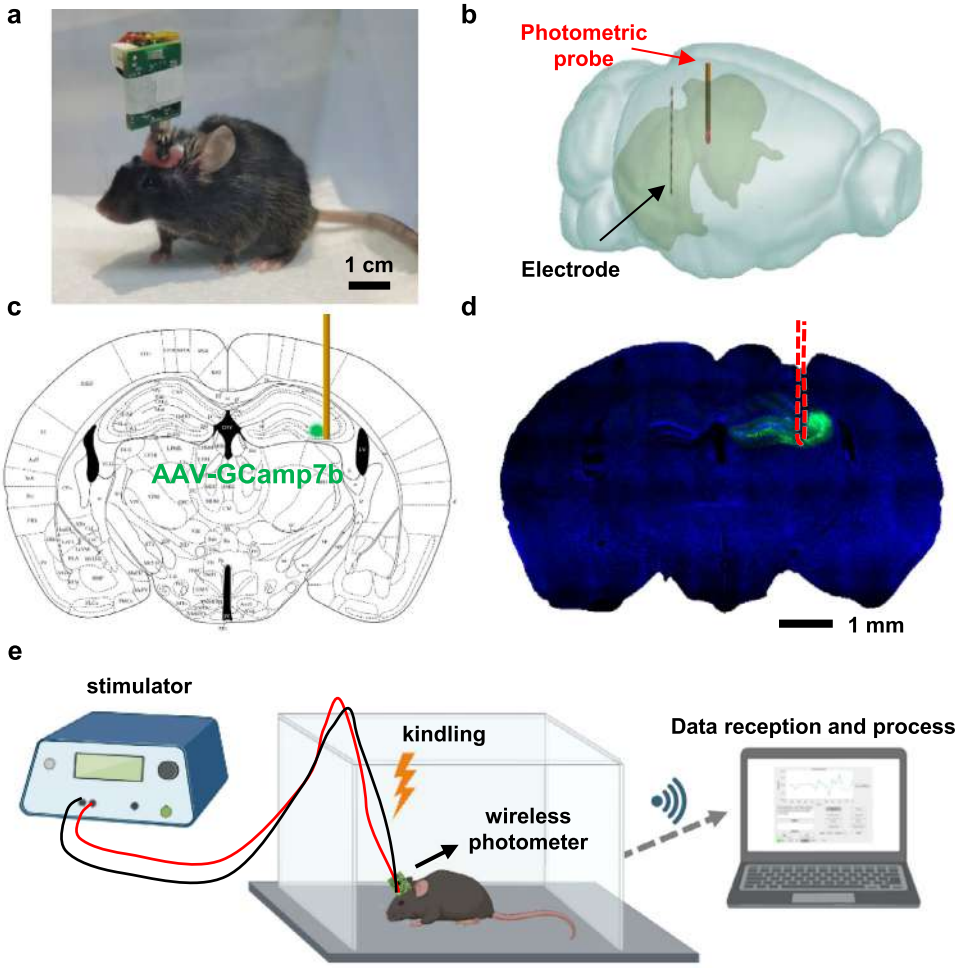

Figure 3. Experimental paradigm of in vivo Ca^{2+} fluorescence recording with the wireless photometric probe. a) Photograph of a freely behaving mouse carrying the wireless module. b) 3D scheme of a mouse brain implanted with a stimulating electrode and a photometric probe in the ipsilateral hippocampus (CA1 and CA3, respectively). c) Schematic illustration of the probe implanted in CA3 expressing jGCaMP7b. d) Fluorescence image showing immunohistochemical staining of nuclei (DAPI, blue) and neurons expressing Ca^{2+} fluorescence (jGCaMP7b, green) after probe implantation for 4 days. Lesion areas are outlined by red dashed lines. e) Schematic diagram showing wireless Ca^{2+} fluorescence recording in mice with kindling (electrical stimulation) induced seizure.

collected ipsilaterally are significantly higher than those recorded contralaterally (Figure 4e).

For comparison, we perform similar experiments for mice with EGFP expression in the hippocampus, which also exhibits green fluorescence under blue excitation but independent of local Ca^{2+} variations (Figure S6a, Supporting Information). Upon kindling, our photometric probes do not capture any obvious fluorescence fluctuations in either the ipsilateral or the contralateral CA3 of these animals (Figure S6b, Supporting Information). These stable output signals collected from EGFP-expressing animals also reveal that electrical stimulations impose negligible artefacts on the photometric probe.

Besides electrical stimulations, drug administrations can also induce seizure activities in various animal models.[65–67] In **Figure 5a**, we record Ca^{2+} signals in the hippocampus (CA3) after intraperitoneally injecting kainic acid (KA) in mice. As a representative trial, Figure 5b presents continuously monitored Ca^{2+} fluorescence collected for ≈1 h following KA administration. Unlike kindling-provoked seizures, KA-induced seizure events occur more randomly and sparsely. 10 individual Ca^{2+} spikes taken from 5 mice are averaged and shown in Figure 5c. These spikes exhibit patterns with durations and amplitudes similar to those elicited by kindlings, most likely due to the fact that they represent synchronized activities from a cluster of neurons in the same brain region (CA3).

3. Discussion

In summary, we develop a wireless photometric probe system to capture fluorescence signals in the brain and demonstrate its ability to detect Ca^{2+} dynamics associated with seizure activities in behaving mice. Compared to fiber-based photometric systems,[46–48] our implantable probe design supports wireless control and integrates microscale optoelectronic devices on the probe to reduce the system's complexity. Furthermore, our probe

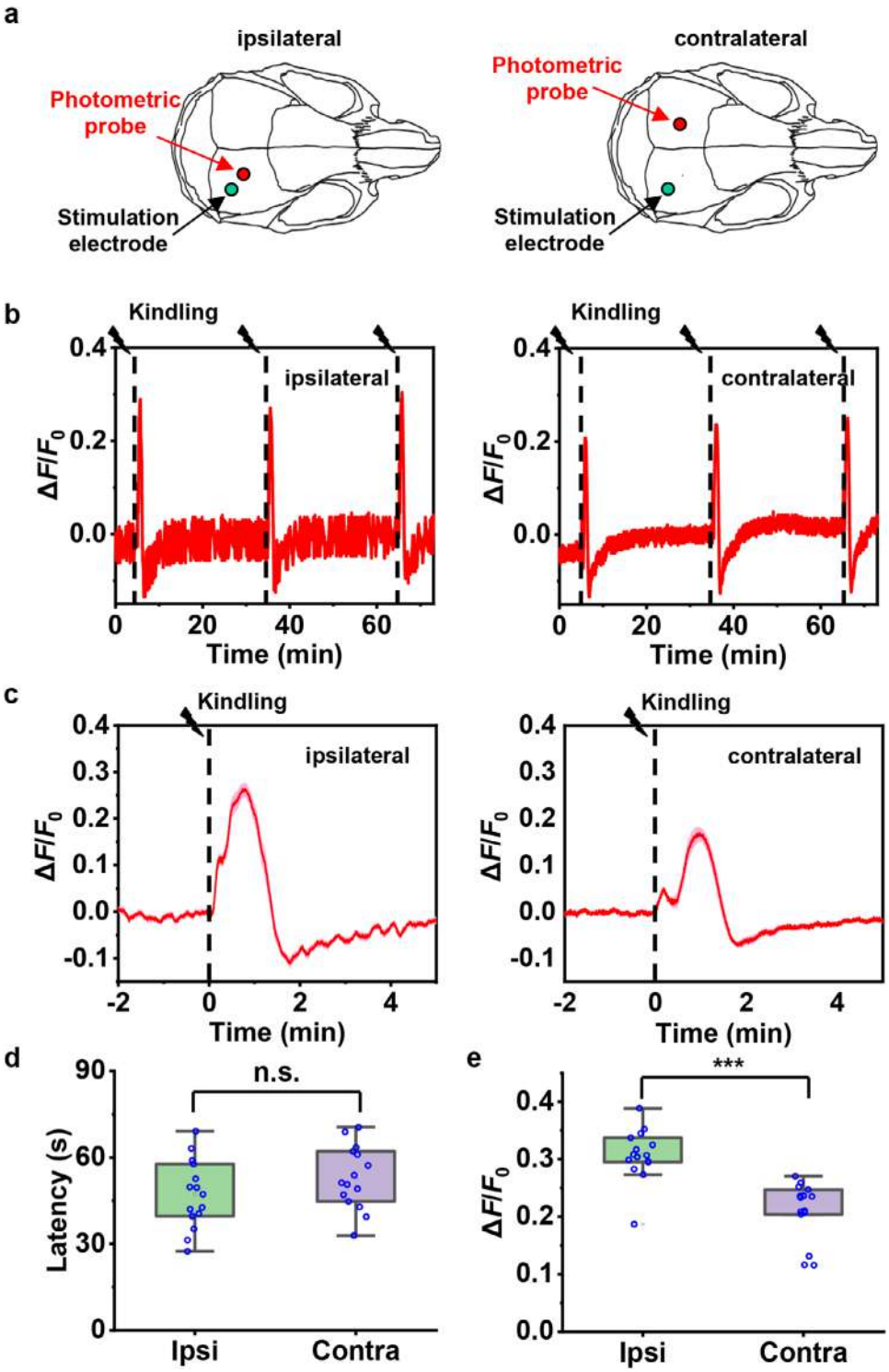

Figure 4. In vivo Ca^{2+} fluorescence recording in the hippocampus (CA3) of mice under electrical stimulation. a) 2D, horizontal-view schematics showing the positions of the photometric probe (CA3) and the stimulation electrode (CA1) implanted in the ipsilateral (left) and the contralateral (right) hippocampus of mice. b) Continuously monitored Ca^{2+} fluorescence in the ipsilateral (left) and the contralateral (right) CA3 during sequential kindling over multiple trials. c) Averaged Ca^{2+} fluorescence spikes responding to kindling in the CA1 recorded in the ipsilateral (left, from 15 individual trials in $n = 3$ mice) and the contralateral (right, from 15 individual trials in $n = 5$ mice) CA3. The solid lines and shaded areas indicate the mean and s.e.m., respectively. d) Comparison of the latency time from kindling in CA1 to reaching the Ca^{2+} fluorescence peaks recorded in the ipsilateral hippocampus and the contralateral CA3. e) Comparison of Ca^{2+} fluorescence peak values recorded in the ipsilateral hippocampus and the contralateral CA3. For (d) and (e), one-way ANOVA and LSD post-hoc comparison are performed, n.s. $p > 0.05$, *** $p < 0.001$. Values are represented as mean ± s.e.m.

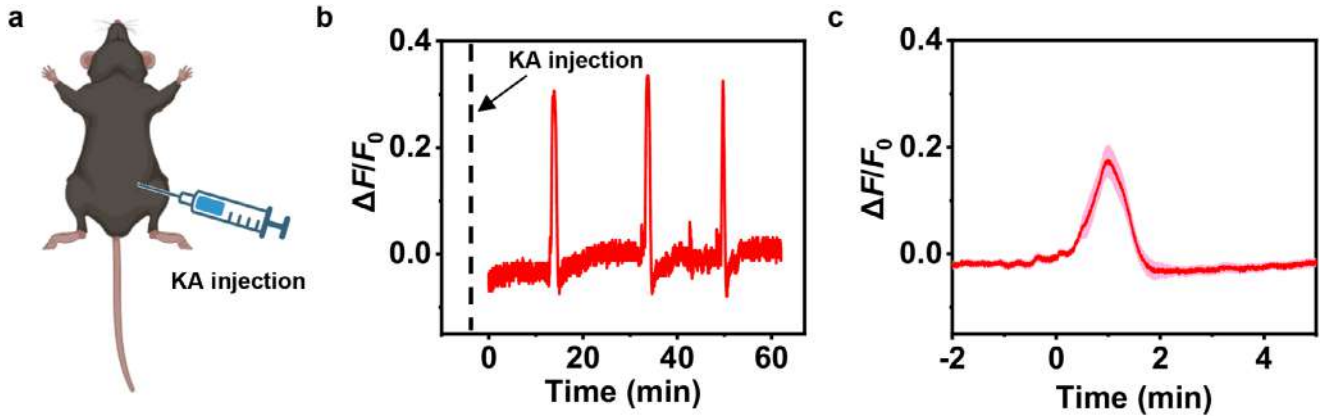

Figure 5. In vivo Ca^{2+} fluorescence recording in the hippocampus (CA3) of mice with seizure induced by medication. a) Schematic diagram showing the seizure model established by injecting kainic acid (KA) into the abdomen of a mouse. b) Continuously monitored Ca^{2+} fluorescence in CA3 after KA administration. c) Averaged Ca^{2+} fluorescence spikes associated with seizure occurrence following KA administration (10 individual trials from $n = 5$ mice). The solid lines and shaded areas indicate the mean and s.e.m., respectively.

implements thin-film micro-LEDs and detectors other than thick chips reported in previously reported photometric probes,[49,50] while spectral-selective filter designs enhance the signal-to-noise ratio. Additionally, Bluetooth modules provide extended communication range and improved data transmission rates. Apart from hippocampus, the probe can be designed to approach many other deep brain regions and investigate corresponding cell-specific Ca^{2+} activities. Although the system's utility is verified in a seizure model involving a single animal, in the future, its capability will be expanded to multiple animals whose Ca^{2+} activities can be simultaneously collected by correctly setting up the corresponding addressable Bluetooth modules.[53] Furthermore, the cooperation of our wireless photometric probe with a camera-based behavioral monitoring system would facilitate the study of more sophisticated social interactions, such as grooming, hierarchies, aggression, courtship, and sexual behaviors.[5,68–72] Integrated arrays of microscale devices and probes can be designed and fabricated to capture neural signals in multiple nuclei and regions.[73–75] We envision that these strategies of device implants and system implementations will find widespread applications in neuroscience research.

4. Experimental Section

Photometric Probe Fabrication: The photometric probe is fabricated by integrating microscale optoelectronic devices through metallization and insulating processes. The probe's detailed structure consists of (from bottom to top) a flexible double-sided copper (Cu)-coated polyimide (PI) substrate (18 μm Cu/25 μm PI/18 μm Cu), an indium gallium nitride (InGaN)-based blue-emitting micro-LED (125 μm × 185 μm × 7 μm), a thin-film shortpass filter (SP495, designed and fabricated by Shenyang Academy of Instrumentation Science CO., LTD.) (150 μm × 220 μm × 6.6 μm), an indium gallium phosphate (InGaP)-based photodetector (140 μm × 195 μm × 7 μm), and a dye filter composed of a mixture of 1 wt.% ABS473 dye and 99 wt.% epoxy SU8-3005 (spin-coated at 500 rpm for 5 s and 3000 rpm for 30 s) (160 μm × 220 μm × 5 μm). Photolithography and transfer technologies are employed during the fabrication process. The probe's shape is defined using laser milling. To enhance insulation and waterproofness, layers of polydimethylsiloxane (PDMS) and Parylene C are coated onto the surface. The detailed fabrication process for these optoelectronic devices is described in the Supporting Information and the previous works.[52,54]

Devices Characterization: Current–voltage (*I–V*) characteristic curves of the micro-LED and the photodetector are measured by a Keithley 2400 sourcemeter. Transmission spectra of the short-pass filter and the dye filter are measured by the spectrophotometer Cary5000. LED irradiances and external quantum efficiencies (EQE) of the detector are measured using a spectroradiometer with an integrating sphere (LabSphere Inc.). An external LED lamp (M530L4-C1, Thorlabs) is also used to test the detector's photo response, and it is powered by a Keysight E3631A triple-output DC power supply.

Wireless Circuit Design: A customized circuit module is designed to support the photometric probe operation. The circuit can be divided into four parts: the microcontroller unit (MCU) module, the power supply module, the LED driver module, and the trans-impedance amplifier module. An nRF52832 chip is chosen as the MCU to control the whole circuit, and the Bluetooth wireless communication function of it provides a wireless modulation method for the photometric system. A built-in analog-to-digital converter (ADC) on the circuit collects the output signal with a sampling rate of 10 Hz. A rechargeable lithium-ion battery with a capacity of 60 mAh and a voltage regulator chip (NCP161) form the power supply module with a stable output voltage of 3.6 V. The micro-LED on the probe is driven by a constant-current chip (LTC3212), with its output current set to 0.4 mA through an external resistor. This configuration yields an optical power output of 10 μW for the LED when the filter is implemented, compared to 40 μW for the LED without a filter. An OPA391 operational amplifier is applied to set up the trans-impedance amplifier module, converting the photocurrent into voltage signals, and the amplifier gain is set to be 50 MΩ through a resistor. The Bluetooth communication system consists of the wireless module as the Bluetooth slave circuit and a dedicated development board (IK-52832DK, Acmemcu) as the Bluetooth master circuit. The master circuit is interfaced with a computer system, enabling operational control of the fluorescence monitoring system via a specifically designed Graphical User Interface (GUI) software application. Video data for animals is analyzed using DeepLabCut, with only tracking points exhibiting a likelihood score > 0.85 retained for plotting.

Animal Preparation: Animal care and all experiments are in accordance with the institutional guidelines of Tsinghua University, with protocols approved by the Institutional Animal Care and Use Committee (IACUC). All animals are socially housed in a 12 h/12 h (7 am – 7 pm) light/dark cycle, with food and water *ad alibitum*. Male B6J mice aged at 9 weeks are used to conduct fluorescent detection tests, by injecting of AAV2/9-hSyn-jGCaMP7b-WPRE-pA virus (2×10^{12}/500 nL) or AAV2/8-hSyn-EGFP-WPRE-pA virus (3×10^{12}/500 nL) into the hippocampus (CA3: AP = −1.80 mm, ML = −1.86 mm, DV = −2.25 mm).

Stereotaxic Surgery: One month after the jGCaMP7b virus injection, the photometric probe and the stimulation electrode are implanted into the mouse brain. Avertin (280 mg per kg body weight) is injected as an anesthetic before the surgery on a mouse. About 5 min after the anesthetization, place the mouse onto the stereotaxic apparatus, preparing for the surgery. Shave the scalp and level the skull before drilling two holes (with a diameter of ≈0.5 mm) in the skull. To collect the fluorescent signals, the photometric probe will be implanted where the jGCaMP7b virus is injected (CA3). After the probe implantation, use dental cement (Super Bond) to fix it. Around 10 min later, implant an acicular tungsten electrode (catalogue no. 796 000, A-M Systems) to CA1 (AP = −2.90 mm, ML = −3.00 mm, DV = −3.20 mm) to induce the mouse seizure. Finally, dental cement is applied to fix the electrode and cover the exposed skull.

Immunohistochemistry: At 4 or 6 days following the stereotaxic surgery, the experimental mice are sacrificed with an overdose of Avertin and transcardially perfused with phosphate buffer solution (PBS) and 4% paraformaldehyde (PFA). The brains are then fixed in 4% PFA for 4 h and 30% sucrose for 24 h, and 40-µm-thick coronal sections are prepared by a cryostat (RWD FS800A). After rinsing the brain slice with PBS, dye the slice and seal the sample for observation. DAPI Sigma D9542 is used for the nucleus dyeing, and it is diluted by 1:10 000 with PBS before applying. Fluorescence-preserving mounting medium (IH0252, LEAGENE) is used as the mounting solution when encapsulating the brain slice. The brain slices are imaged through the Olympus IXplore spinning disk microscope.

To compare the difference of the probe tip position at day 1 and day 21 after the stereotaxic surgery, after the perfusion and slicing step, the brain slices are washed for three 5-min sessions with PBS (1×, 4 °C) before being incubated in a sodium citrate solution (0.01 mol L^{-1} in H_2O) for antigen retrieval. The slices are washed again for three 5-min sessions, incubated in a blocking solution, permeabilized (0.3% Triton X-100 and 5% normal goat serum (Servicebio) in PBS) for 1 h at room temperature, and washed again for three 5-min sessions. Then the slices are first incubated in PBST (1× PBS with 0.3% Triton X-100) with primary antibodies overnight at 4 °C for astrocytes (anti-GFAP mouse mAb, GB12090, 1:1000, Servicebio) and microglia (anti-IBA-1 rabbit pAb, GB11105, Servicebio). The slices are then washed with PBS and incubated with secondary antibodies for 1 h at room temperature (Alexa Fluor 488-conjugated Goat Anti-Rabbit IgG, GB25303, 1:1000, Servicebio; Cy3 conjugated Goat Anti-mouse IgG, GB21301, 1:1000, Servicebio) followed by DAPI (1:1000, Sigma-Aldrich) for 20 min. After staining, the slices are mounted with a glass coverslip and Fluoromount-G (0100-01, SouthernBiotech) before imaging.

Statistical Analysis: The fluorescence signal change is quantified as $\Delta F/F_0$, where F_0 represents the baseline fluorescence response. For in vitro measurements, F_0 was determined at 0 Ca^{2+} concentration, with ΔF calculated as the difference between measured fluorescence (F) and F_0. In vivo experiments defined F_0 as the average response from 2 min pre-kindling to 5 min post-kindling, with ΔF similarly derived. Data are presented as mean ± s.e.m. In vitro Ca^{2+} fluorescence changes ($\Delta F/F_0$) were obtained from three independent replicates (n = 3 probes per condition). For in vivo recordings, kindling-evoked Ca^{2+} fluorescence spikes responding to kindling in the CA1 were analyzed from 15 trials in n = 3 mice (ipsilateral CA3) and 15 trials in n = 5 mice (contralateral CA3). Statistical comparisons of both response latency (kindling-to-peak) and peak amplitude between ipsilateral hippocampal and contralateral CA3 recordings were performed using one-way ANOVA with LSD post-hoc tests, with significance thresholds set at $^{***}p < 0.001$ and n.s. (not significant) for $p > 0.05$. All analyses were conducted using Origin 2019b (64-bit version), with values reported as mean ± s.e.m.

Supporting Information

Supporting Information is available from the Wiley Online Library or from the author.

Acknowledgements

This work is supported by the National Natural Science Foundation of China (NSFC) (T2425003 and 52272277, to X.S.; 62404032 to L.L.; T2122010 and 52171239 to L.Y., 62422501 to H.D.), Beijing Nova Program (20240484742 to H.D.). The authors acknowledge characterization work supported by the Center of Intelligent Sensing and Precise Testing Technology in Optics and Photonics, Beijing Institute of Technology, and Tsinghua Nanofabrication Technology Center. [Correction added on November 24, 2025, after first online publication: Section 2.4 has been updated. Correction added on January 19, 2026, after first online publication: supplementary information has been updated.]

Conflict of Interest

The authors declare no conflict of interest.

Data Availability Statement

The data that support the findings of this study are available from the corresponding author upon reasonable request.

Keywords

calcium fluorescence, implantable devices, optoelectronic devices, seizure

Received: March 7, 2025
Revised: June 19, 2025
Published online: October 4, 2025

[1] A. Selimbeyoglu, C. K. Kim, M. Inoue, S. Y. Lee, A. S. O. Hong, I. Kauvar, C. Ramakrishnan, L. E. Fenno, T. J. Davidson, M. Wright, K. Deisseroth, *Sci. Transl. Med.* **2017**, *9*, aah6733.
[2] M. Sato, N. Nakai, S. Fujima, K. Y. Choe, T. Takumi, *Mol. Psychiatry* **2023**, *28*, 3194.
[3] C. E. Stafstrom, L. Carmant, *Perspect. Med.* **2015**, *5*, a022426.
[4] L. X. Cai, K. Pizano, G. W. Gundersen, C. L. Hayes, W. T. Fleming, S. Holt, J. M. Cox, I. B. Witten, *Elife* **2020**, *9*, 54936.
[5] Y. Yoon, H. Shin, D. Byun, J. Woo, Y. Cho, N. Choi, I. J. Cho, *Nat. Commun.* **2022**, *13*, 5521.
[6] K. D. Wise, J. B. Angell, A. Starr, *IEEE Trans. Biomed. Eng.* **1970**, *17*, 238.
[7] J. J. Jun, N. A. Steinmetz, J. H. Siegle, D. J. Denman, M. Bauza, B. Barbarits, A. K. Lee, C. A. Anastassiou, A. Andrei, C. Aydin, M. Barbic, T. J. Blanche, V. Bonin, J. Couto, B. Dutta, S. L. Gratiy, D. A. Gutnisky, M. Hausser, B. Karsh, P. Ledochowitsch, C. M. Lopez, C. Mitelut, S. Musa, M. Okun, M. Pachitariu, J. Putzeys, P. D. Rich, C. Rossant, W. L. Sun, K. Svoboda, et al., *Nature* **2017**, *551*, 232.
[8] Z. Zhao, H. Zhu, X. Li, L. Sun, F. He, J. E. Chung, D. F. Liu, L. Frank, L. Luan, C. Xie, *Nat. Biomed. Eng.* **2023**, *7*, 520.
[9] E. M. Maynard, C. T. Nordhausen, R. A. Normann, *Electroencephalogr. Clin. Neurophysiol.* **1997**, *102*, 228.
[10] T. Xiao, F. Wu, J. Hao, M. Zhang, P. Yu, L. Mao, *Anal. Chem.* **2017**, *89*, 300.
[11] J. G. Roberts, L. A. Sombers, *Anal. Chem.* **2018**, *90*, 490.
[12] M. A. Booth, S. A. Gowers, C. L. Leong, M. L. Rogers, I. C. Samper, A. P. Wickham, M. G. Boutelle, *Anal. Chem.* **2018**, *90*, 2.
[13] A. Tooker, T. E. Madsen, A. Yorita, A. Crowell, K. G. Shah, S. Felix, H. S. Mayberg, S. Pannu, D. G. Rainnie, V. Tolosa, *IEEE EMBC* **2013**, *2013*, 5159.

[14] Y. Liu, A. T. L. Leong, Y. Zhao, L. Xiao, H. K. F. Mak, A. C. O. Tsang, G. K. K. Lau, G. K. K. Leung, E. X. Wu, *Nat. Commun.* **2021**, *12*, 7238.
[15] D. Sulzer, C. Cassidy, G. Horga, U. J. Kang, S. Fahn, L. Casella, G. Pezzoli, J. Langley, X. P. Hu, F. A. Zucca, I. U. Isaias, L. Zecca, *npj Parkinson's Disease* **2018**, *4*, 11.
[16] J. E. Chen, G. H. Glover, *Neuropsychol. Rev.* **2015**, *25*, 289.
[17] A. Ranft, D. Golkowski, T. Kiel, V. Riedl, P. Kohl, G. Rohrer, J. Pientka, S. Berger, A. Thul, M. Maurer, C. Preibisch, C. Zimmer, G. A. Mashour, E. F. Kochs, D. Jordan, R. Ilg, *Anesthesiology* **2016**, *125*, 861.
[18] K. N. Sheth, M. H. Mazurek, M. M. Yuen, B. A. Cahn, J. T. Shah, A. Ward, J. A. Kim, E. J. Gilmore, G. J. Falcone, N. Petersen, K. T. Gobeske, F. Kaddouh, D. Y. Hwang, J. Schindler, L. Sansing, C. Matouk, J. Rothberg, G. Sze, J. Siner, M. S. Rosen, S. Spudich, W. T. Kimberly, *JAMA Neurol.* **2020**, *78*, 41.
[19] G. Cui, S. B. Jun, X. Jin, G. Luo, M. D. Pham, D. M. Lovinger, S. S. Vogel, R. M. Costa, *Nat. Protoc.* **2014**, *9*, 1213
[20] T. H. Kim, Y. Zhang, J. Lecoq, J. C. Jung, J. Li, H. Zeng, C. M. Niell, M. J. Schnitzer, *Cell Rep.* **2016**, *17*, 3385.
[21] L. V. Doronina-Amitonova, I. V. Fedotov, O. I. Ivashkina, M. A. Zots, A. B. Fedotov, K. V. Anokhin, A. M. Zheltikov, *Sci. Rep.* **2013**, *3*, 3265.
[22] R. Liang, G. J. Broussard, L. Tian, *ACS Chem. Neurosci.* **2015**, *6*, 84.
[23] E. Belykh, N. L. Martirosyan, K. Yagmurlu, E. J. Miller, J. M. Eschbacher, M. Izadyyazdanabadi, L. A. Bardonova, V. A. Byvaltsev, P. Nakaji, M. C. Preul, *Front. Surg.* **2016**, *3*, 55.
[24] M. Kannan, G. Vasan, C. Huang, S. Haziza, J. Z. Li, H. Inan, M. J. Schnitzer, V. A. Pieribone, *Nat. Methods* **2018**, *15*, 1108.
[25] E. A. Specht, E. Braselmann, A. E. Palmer, *Annu. Rev. Physiol.* **2017**, *79*, 93.
[26] H. J. Cha, C. Wu, J. J. Valdes, G. Rao, W. E. Bentley, *Biotechnol. Bioeng.* **2000**, *67*, 565.
[27] J. Wiedenmann, B. Vallone, F. Renzi, K. Nienhaus, S. Ivanchenko, C. Rocker, G. U. Nienhaus, *J. Biomed. Opt.* **2005**, *10*, 014003.
[28] W. B. Frommer, M. W. Davidson, R. E. Campbell, *Chem. Soc. Rev.* **2009**, *38*, 2833.
[29] A. S. Mishin, V. V. Belousov, K. M. Solntsev, K. A. Lukyanov, *Curr. Opin. Chem. Biol.* **2015**, *27*, 1.
[30] M. Nampally, B. M. Moerschbacher, S. Kolkenbrock, *Appl. Environ. Microbiol.* **2012**, *78*, 3114.
[31] J. R. Enterina, L. Wu, R. E. Campbell, *Curr. Opin. Chem. Biol.* **2015**, *27*, 10.
[32] H. J. Koester, B. Sakmann, *The Journal of Physiology* **2000**, *529*, 625.
[33] H. R. Parri, T. M. Gould, V. Crunelli, *Nat. Neurosci.* **2001**, *4*, 803.
[34] C. Grienberger, A. Konnerth, *Neuron* **2012**, *73*, 862.
[35] F. Ali, A. C. Kwan, *Neurophotonics* **2020**, *7*, 011402.
[36] J. Nakai, M. Ohkura, K. Imoto, *Nat. Biotechnol.* **2001**, *19*, 137.
[37] J. Akerboom, T. W. Chen, T. J. Wardill, L. Tian, J. S. Marvin, S. Mutlu, N. C. Calderon, F. Esposti, B. G. Borghuis, X. R. Sun, A. Gordus, M. B. Orger, R. Portugues, F. Engert, J. J. Macklin, A. Filosa, A. Aggarwal, R. A. Kerr, R. Takagi, S. Kracun, E. Shigetomi, B. S. Khakh, H. Baier, L. Lagnado, S. S. Wang, C. I. Bargmann, B. E. Kimmel, V. Jayaraman, K. Svoboda, D. S. Kim, et al., *J. Neurosci.* **2012**, *32*, 13819.
[38] C. Stringer, M. Pachitariu, *Curr. Opin. Neurobiol.* **2019**, *55*, 22.
[39] M. Tada, A. Takeuchi, M. Hashizume, K. Kitamura, M. Kano, *Eur. J. Neurosci.* **2014**, *39*, 1720.
[40] N. Takahashi, T. Sasaki, A. Usami, N. Matsuki, Y. Ikegaya, *Neurosci. Res.* **2007**, *58*, 219.
[41] T. P. Patel, K. Man, B. L. Firestein, D. F. Meaney, *J. Neurosci. Methods* **2015**, *243*, 26.
[42] M. Sakamoto, T. Yokoyama, *Neurosci. Res.* **2025**, *15*, 56.
[43] J. Wu, Y. Liang, S. Chen, C. L. Hsu, M. Chavarha, S. W. Evans, D. Shi, M. Z. Lin, K. K. Tsia, N. Ji, *Nat. Methods* **2020**, *17*, 287.
[44] N. Ji, *Nat. Methods* **2017**, *14*, 374.
[45] C. M. Hobson, M. Guo, H. D. Vishwasrao, Y. Wu, H. Shroff, T. L. Chew, *Nat. Methods* **2022**, *19*, 1538.
[46] Y. Li, L. Zhan, Y. Wang, R. Chen, X. Yang, X. Wu, Y. Wang, H. Chen, C. Xu, W. Pei, *Sens. Actuators, A* **2021**, *331*, 112948.
[47] F. Pisano, M. Pisanello, S. J. Lee, J. Lee, E. Maglie, A. Balena, L. Sileo, B. Spagnolo, M. Bianco, M. Hyun, M. De Vittorio, B. L. Sabatini, F. Pisanello, *Nat. Methods* **2019**, *16*, 1185.
[48] Y. Sych, M. Chernysheva, L. T. Sumanovski, F. Helmchen, *Nat. Methods* **2019**, *16*, 553.
[49] L. Lu, P. Gutruf, L. Xia, D. L. Bhatti, X. Wang, A. Vazquez-Guardado, X. Ning, X. Shen, T. Sang, R. Ma, G. Pakeltis, G. Sobczak, H. Zhang, D. O. Seo, M. Xue, L. Yin, D. Chanda, X. Sheng, M. R. Bruchas, J. A. Rogers, *Proc. Natl. Acad. Sci. U.S.A.* **2018**, *115*, E1374.
[50] A. Burton, S. N. Obaid, A. Vazquez-Guardado, M. B. Schmit, T. Stuart, L. Cai, Z. Chen, I. Kandela, C. R. Haney, E. A. Waters, H. Cai, J. A. Rogers, L. Lu, P. Gutruf, *Proc. Natl. Acad. Sci. U.S.A.* **2020**, *117*, 2835.
[51] X. Sheng, C. J. Corcoran, J. He, L. Shen, S. Kim, J. Park, R. G. Nuzzo, J. A. Rogers, *Phys. Chem. Chem. Phys.* **2013**, *15*, 20434.
[52] L. Li, C. Liu, Y. Su, J. Bai, J. Wu, Y. Han, Y. Hou, S. Qi, Y. Zhao, H. Ding, Y. Yan, L. Yin, P. Wang, Y. Luo, X. Sheng, *Adv. Mater. Technol.* **2018**, *3*, 1700239.
[53] X. Cai, H. Zhang, P. Wei, Q. Liu, D. Sheng, Z. Li, B. Zhang, G. Tang, W. Zhao, Z. Ye, Z. Xue, Y. Xie, Y. Dai, C. Wang, Y. Wang, X. Fu, L. Yin, H. Peng, H. Ding, G. Zhao, X. Sheng, *Nat. Photonics* **2024**, *18*, 492.
[54] C. Liu, Q. Zhang, D. Wang, G. Zhao, X. Cai, L. Li, H. Ding, K. Zhang, H. Wang, D. Kong, L. Yin, L. Liu, G. Zou, L. Zhao, X. Sheng, H. Performance, *Adv. Opt. Mater.* **2018**, *6*, 1800146.
[55] S. N. Obaid, N. Quirion, J. D. T. Balansag, N. Daza, X. Shi, Z. Chen, L. Lu, *ACS Appl. Electron. Mater.* **2023**, *5*, 1688.
[56] S. Murugalakshmi, *J. Mobile Appl. Technol.* **2023**, *10*, 31.
[57] Y. Zhang, M. Rozsa, Y. Liang, D. Bushey, Z. Wei, J. Zheng, D. Reep, G. J. Broussard, A. Tsang, G. Tsegaye, S. Narayan, C. J. Obara, J. X. Lim, R. Patel, R. Zhang, M. B. Ahrens, G. C. Turner, S. S. Wang, W. L. Korff, E. R. Schreiter, K. Svoboda, J. P. Hasseman, I. Kolb, L. L. Looger, *Nature* **2023**, *615*, 884.
[58] M. A. García, S. E. Paje, M. A. Villegas, J. Llopis, *Appl. Phys. A* **2014**, *74*, 83.
[59] G. Mouri, E. Jimenez-Mateos, T. Engel, M. Dunleavy, S. Hatazaki, A. Paucard, S. Matsushima, W. Taki, D. C. Henshall, *Brain Res.* **2008**, *1213*, 140.
[60] J. S. Mueller, F. C. Tescarollo, T. Huynh, D. A. Brenner, D. J. Valdivia, K. Olagbegi, S. Sangappa, S. C. Chen, H. Sun, *Nat. Commun.* **2023**, *14*, 6010.
[61] X. Yan, J. Liu, J. Huang, M. Huang, F. He, Z. Ye, W. Xiao, X. Hu, Z. Luo, *Neurochem. Res.* **2014**, *39*, 129.
[62] P. Zhou, F. He, Y. Han, B. Liu, S. Wei, *Bioelectrochemistry* **2018**, *124*, 7.
[63] V. S. Alves, H. S. Alves-Silva, D. J. B. Orts, L. Ribeiro-Silva, M. Arcisio-Miranda, F. A. Oliveira, *Neuroscience* **2019**, *421*, 95.
[64] J. K. Trevathan, A. J. Asp, E. N. Nicolai, J. Trevathan, N. A. Kremer, T. D. Y. Kozai, D. Cheng, M. Schachter, J. J. Nassi, S. L. Otte, J. G. Parker, J. L. Lujan, K. Ludwig, *J. Neural Eng.* **2020**, *18*, 026008.
[65] B. J. Albala, S. L. Moshe, R. Okada, *Brain Res.* **1984**, *315*, 139.
[66] G. Sperk, H. Lassmann, H. Baran, S. J. Kish, F. Seitelberger, O. Hornykiewicz, *Neuroscience* **1983**, *10*, 1301.
[67] E. Rusina, C. Bernard, A. Williamson, *eNeuro* **2021**, *8*, 1.
[68] D. B. Piza, B. W. Corrigan, R. A. Gulli, S. Do Carmo, A. C. Cuello, L. Muller, J. Martinez-Trujillo, *Nat. Commun.* **2024**, *15*, 4053.
[69] E. A. Naumann, A. R. Kampff, D. A. Prober, A. F. Schier, F. Engert, *Nat. Neurosci.* **2010**, *13*, 513.
[70] T. Ninomiya, A. Noritake, M. Ullsperger, M. Isoda, *Neurosci. Res.* **2018**, *137*, 1.
[71] M. Ullsperger, A. G. Fischer, R. Nigbur, T. Endrass, *Trends Cogn. Sci.* **2014**, *18*, 259.

[72] L. Kingsbury, S. Huang, J. Wang, K. Gu, P. Golshani, Y. E. Wu, W. Hong, *Cell* **2019**, *178*, 429.
[73] M. E. Obien, K. Deligkaris, T. Bullmann, D. J. Bakkum, U. Frey, *Frontiers in Neuroscience* **2014**, *8*, 423.
[74] N. A. Steinmetz, C. Aydin, A. Lebedeva, M. Okun, M. Pachitariu, M. Bauza, M. Beau, J. Bhagat, C. Bohm, M. Broux, S. Chen, J. Colonell, R. J. Gardner, B. Karsh, F. Kloosterman, D. Kostadinov, C. Mora-Lopez, J. O'Callaghan, J. Park, J. Putzeys, B. Sauerbrei, R. J. J. van Daal, A. Z. Vollan, S. Wang, M. Welkenhuysen, Z. Ye, J. T. Dudman, B. Dutta, A. W. Hantman, K. D. Harris, et al., *Science* **2021**, *372*, abf4588.
[75] J. Viventi, D. H. Kim, L. Vigeland, E. S. Frechette, J. A. Blanco, Y. S. Kim, A. E. Avrin, V. R. Tiruvadi, S. W. Hwang, A. C. Vanleer, D. F. Wulsin, K. Davis, C. E. Gelber, L. Palmer, J. Van der Spiegel, J. Wu, J. Xiao, Y. Huang, D. Contreras, J. A. Rogers, B. Litt, *Nat. Neurosci.* **2011**, *14*, 1599.

Supporting Information

Device fabrication

The detailed structure of our proposed photometric probe involves (from bottom to top): a flexible double side copper (Cu) coated polyimide (PI) (18 μm Cu / 25 μm PI / 18 μm Cu) substrate, an indium gallium nitride (InGaN) based blue emitting micro-LED (size: 125 μm × 185 μm × 7 μm), a thin-film shortpass filter (SP495) (size: 150 μm × 220 μm × 6.6 μm), an indium gallium phosphate (InGaP) based photodetector (size: 140 μm × 195 μm × 7 μm), a dye filter made from a mixture of 1 wt% ABS473 dye and 99 wt% epoxy SU8-3005 (500 rpm/ 5 s, 4000 rpm/ 30 s) (size: 160 μm × 220 μm × 5 μm).

A detailed description of the fabrication of implantable fluorescent photometric probe in detail:

Micro-LED fabrication

The fabrication of the thin-film micro-LEDs follow the procedure outlined in our previous work. The structure is grown on sapphire substrates using metalorganic chemical vapor deposition (MOCVD). Freestanding micro-LEDs are obtained through laser lift-off using a KrF excimer laser (248 nm). Polydimethylsiloxane (PDMS)-based stamps are employed to transfer the released micro-LEDs onto the sample substrates.

Reference: Li, L. et al. Heterogeneous Integration of Microscale GaN Light-Emitting Diodes and Their Electrical, Optical, and Thermal Characteristics on Flexible Substrates. *Advanced Materials Technologies* **3**, 1700239 (2018).

Photodetector fabrication

The InGaP based photodetector structure is grown on gallium arsenide (GaAs) substrates via metalorganic chemical vapor deposition (MOCVD). The epitaxial structure of the wafer is displayed in **Table S1**. The material of each layer from top to bottom: a layer of 500 nm n-type $(Al_{0.7}Ga_{0.3})_{0.5}In_{0.5}P$ filter (Si-doped, 2×10^{18} cm^{-3}), a layer of 10 nm n-type GaAs contact (Si-doped, $> 6 \times 10^{18}$ cm^{-3}), a layer of 30 nm n-type $In_{0.5}Al_{0.25}Ga_{0.25}P$ window (Si-doped, 5×10^{18} cm^{-3}), a layer of 100 nm n-type $In_{0.5}Ga_{0.5}P$ emitter (Si-doped, 2×10^{18} cm^{-3}), a layer of 1 μm p-type $In_{0.5}Ga_{0.5}P$ base (Zn-doped, 3×10^{16} cm^{-3}), a layer of 100 nm p-type $In_{0.5}Ga_{0.5}P$ back-surface field (BSF) (Mg-doped, 2×10^{18} cm^{-3}), a layer of 100 nm p-type GaAs contact (Mg-doped, $> 5 \times 10^{18}$ cm^{-3}), a layer of 1 μm p-type $In_{0.5}Ga_{0.5}P$ support (Mg-doped, 2×10^{18} cm^{-3}) and a layer of 500 nm undoped $Al_{0.95}Ga_{0.05}As$ sacrificial on a GaAs substrate.

A description of the fabrication of the photodetectors in detail:

1. Clean up the epitaxial wafer with acetone, isopropyl alcohol (IPA), and deinoized (DI) water.
2. Dehydrate at 110 ℃ for 10 min.

3. Spin coat positive photoresist (PR) (SPR220-v3.0, Microchem, 500 rpm / 6 s, 3000 rpm / 30 s), and soft-bake at 110 ℃ for 1.5 min.
4. Expose PR with a UV lithography machine (URE-2000/25, IOE CAS) with a dose of 150 mJ/cm^2 through a chrome mask, post-bake at 110 ℃ for 1.5 min.
5. Develop PR in an aqueous base developer (AZ300 MIF) for 1 min. Shake it at 20 seconds after the sample is placed in. Rinse with DI water and hard-back at 110 ℃ for 30 min.
6. Etch the 500 nm $(Al_{0.7}Ga_{0.3})_{0.5}In_{0.5}P$ filter layer with a mixture of H_3PO_4 and HCl (1 : 1 by volume) for 9 s, and shake to remove bubbles. Rinse with DI water.
7. Etch the 10 nm GaAs layer with a mixture of H_3PO_4, H_2O_2, and H_2O (3 : 1 : 25 by volume) for 20 s and rinse with DI water.
8. Remove the PR with acetone, rinse with IPA and DI water.
9. Dehydrate at 110 ℃ for 10 min.
10. Spin coat positive photoresist (PR) (SPR220-v3.0, Microchem, 500 rpm / 6 s, 3000 rpm / 30 s), and soft-bake at 110 ℃ for 1.5 min.
11. Expose PR with a UV lithography machine (URE-2000/25, IOE CAS) with a dose of 150 mJ/cm^2 through a chrome mask, post-bake at 110 ℃ for 1.5 min.
12. Develop PR in an aqueous base developer (AZ300 MIF) for 1 min. Shake it at 20 seconds after the sample is placed in. Rinse with DI water and hard-back at 110 ℃ for 30 min.
13. Etch the 30 nm n-type $In_{0.5}Al_{0.25}Ga_{0.25}P$ window layer, the 100 nm n-type $In_{0.5}Ga_{0.5}P$ emitter layer, the 1 μm p-type $In_{0.5}Ga_{0.5}P$ base and the 100 nm p-type

$In_{0.5}Ga_{0.5}P$ BSF layer with a concentrated solution of HCl for ~20 s and rinse with DI water.

14. Remove the PR with acetone, rinse with IPA and DI water.
15. Dehydrate at 110 ℃ for 10 min.
16. Spin coat negative photoresist (NR) (AZ nLOF 2070, MicroChemicals, 500 rpm 6 s, 3000 rpm 30 s) and soft-bake at 110 ℃ for 2 min.
17. Expose NR with a UV lithography machine (URE-2000/25, IOE CAS) with a dose of 45 mJ/cm^2 through a chrome mask, post-bake at 110 ℃ for 1 min..
18. Develop NR in an aqueous base developer (AZ300 MIF) for 1 min. Shake it at 50 seconds after the sample is placed in. Rinse with DI water.
19. Sputter 6 nm / 200 nm of Cr / Au as electrodes.
20. Lift-off in acetone, and clean the sample with acetone, IPA and DI water.
21. Dehydrate at 110 ℃ for 10 min.
22. Pattern PR (SPR220-v3.0, Microchem).
23. Etch the 100 nm p-type GaAs contact layer with a mixture of H_3PO_4, H_2O_2, and H_2O (3 : 1 : 25 by volume) for ~40 s and rinse with DI water.
24. Etch the 1 μm p-type $In_{0.5}Ga_{0.5}P$ support layer with a mixture of concentrated HCl solution and anhydrous ethanol (10 : 1 by volume) for ~60 s until the surface becomes clean.
25. Remove the PR with acetone, rinse with IPA and DI water.
26. Dehydrate at 110 ℃ for 10 min.
27. Pattern PR (SPR220-v3.0, Microchem).

28. Etch the 500 nm undoped $Al_{0.95}Ga_{0.05}As$ sacrificial layer with a mixture of HF solution and H_2O (1 : 10 by volume) for ~2.5 h and rinse with DI water.

Thin-film filter fabrication

The thin-film filters are custom shortpass filters (SP495). The shape is defined by femtosecond laser-cutting (800 nm, Ti-sapphire laser system, Coherent Inc.). The GaAs substrate of the filter is removed after laser cutting in a solution of NH_4OH, H_2O_2 and H_2O (1 : 1 : 2 by volume) for approximately 8 hours. At last, PDMS-based stamps (Sylgard 184 from Dow Corning) are employed to transfer the released filters onto the sample substrates.

Reference: Liu, C. et al. High Performance, Biocompatible Dielectric Thin‐Film Optical Filters Integrated with Flexible Substrates and Microscale Optoelectronic Devices. *Advanced Optical Materials* **6**, 1800146 (2018).

Substrate preparation

1. Cut the copper-clad PI substrate (18 μm Cu / 25 μm PI / 18 μm Cu, DuPont) into a size of 1.5 × 1.8 cm^2.
2. Cut the glass chip into a size of 2 × 2.5 cm^2.
3. Prepare poly(dimethylsiloxane) (PDMS, Sylgard 184, pre-polymer : curing agent = 10:1, by weight) as adhesive.
4. Clean up the glass chip with acetone, IPA, and DI water.

5. Dehydrate at 110 ℃ for 10 min.
6. Spin coat PDMS onto the glass chips (500 rpm 6 s, 3000 rpm 30 s), and soft-bake at 110 ℃ for ~35 s.
7. Laminate PI substrate on the glass and bake up at 110 ℃ for 30 min.
8. Clean up the sample with acetone, IPA, and DI water.
9. Dehydrate at 110 ℃ for 10 min.
10. Spin cast 8 μm thick polyimide (YDPI-102, YiDun New Material Suzhou, 500 rpm 9 s, 3000 rpm 30 s) to form an insulating film.
11. Bake up the sample at 80 ℃, 130 ℃, 180 ℃ and 230 ℃ respectively. The first three temperature steps last for 1 h, and the last temperature step lasts for 2 h.

Marker formation

12. Clean up the sample with acetone, IPA, and DI water.
13. Dehydrate at 110 ℃ for 10 min.
14. Spin coat NR (AZ nLOF 2070, MicroChemicals, 500 rpm 6 s, 3000 rpm 30 s) and soft-bake at 110 °C for 2 min.
15. Pattern the devices position marker through UV lithography with a dose of 45 mJ/cm^2, and post-bake at 110 ℃ for 1 min.
16. Develop in an aqueous base developer (AZ300 MIF) for 1 min. Shake it at 50 seconds after the sample is placed in. Rinse with DI water.
17. Sputter 50 nm Al.
18. Lift-off in acetone, and clean the sample with acetone, IPA and DI water

Micro-LED transfer

19. Clean up the sample with acetone, IPA, and DI water.

20. Dehydrate at 110 ℃ for 10 min.
21. Expose the sample to ultraviolet induced ozone (UV Ozone) for 15 min.
22. Spin coat SU8-3005 epoxy (500 rpm × 9 s, 3000 rpm × 30 s) and soft-bake at 110 ℃ for ~10 s.
23. Transfer print the blue micro-LED onto the sample with PDMS stamps.
24. Expose the sample with UV lithography machine with a dose of 150 mJ/cm^2, and post-bake at 65 ℃ for 1 min and 95 ℃ for 3 min.
25. Hard bake at 110 ℃ for 30 min.

Micro-LED encapsulation

26. Clean up the sample with acetone, IPA, and DI water and dehydrate at 110 ℃ for 10 min.
27. Expose the sample under UV ozone for 15 min.
28. Spin coat SU8-3005 epoxy onto the sample (500 rpm × 9 s, 3000 rpm × 30 s) and soft-bake at 65 ℃ for 1 min and 95 ℃ for 3 min.
29. Expose the electrodes on the LED by UV lithography with a dose of 150 mJ/cm^2, and post-bake at 65 ℃ for 1 min and 95 ℃ for 3 min.
30. Develop in propylene glycol monomethyl ether acetate (PGMEA) for 2.5 min and rinse with IPA.
31. Hard bake at 110 ℃ for 30 min.

Micro-LED metallization

32. Clean up the sample with acetone, IPA, and DI water and dehydrate at 110 ℃ for 10 min.
33. Spin coat AZ nLOF 2070 photoresist (500 rpm 9 s, 3000 rpm 30 s) and soft-bake at 110 ℃ for 2 min.
34. Pattern the conducting wires by UV lithography with a dose of 45 mJ/cm^2, and post-bake at 110 ℃ for 1 min.
35. Develop in an aqueous base developer (AZ300 MIF) for 1 min. Shake it for 50 seconds after the sample is placed in. Rinse with DI water.
36. Deposit 10 nm Cr / 600 nm Cu / 200 nm Au as the conducting wires.
37. Lift-off in acetone, and clean the sample with acetone, IPA and DI water.

Thin-film filter transfer

38. Clean up the sample with acetone, IPA, and DI water and dehydrate at 110 ℃ for 10 min.
39. Expose the sample under UV ozone for 15 min.
40. Spin coat SU8-3005 epoxy (500 rpm 9 s, 3000 rpm 30 s) and soft-bake at 110 ℃ for ~10 s.
41. Transfer print the thin-film filter onto the sample with PDMS stamps.
42. Expose the contact pads of LED by UV lithography with a dose of 150 mJ/cm^2, and post-bake at 65 ℃ for 1 min and 95 ℃ for 3 min.
43. Develop in PGMEA for 2.5 min and rinse with IPA.
44. Hard bake at 110 ℃ for 30 min.

Insulating layer formation

45. Clean up the sample with acetone, IPA, and DI water and dehydrate at 110 ℃ for 10 min.
46. Expose the sample under UV ozone for 15 min.
47. Spin coat SU8-3005 epoxy onto the sample (500 rpm 9 s, 3000 rpm 30 s) and soft-bake at 65 ℃ for 1 min and 95 ℃ for 3 min.
48. Pattern SU8-3005 epoxy to expose contact pads of LED by UV lithography with a dose of 150 mJ/cm^2, and post-bake at 65 ℃ for 1 min and 95 ℃ for 3 min.
49. Develop in PGMEA for 2.5 min and rinse with IPA.
50. Hard bake at 110 ℃ for 30 min.

Micro photodetector transfer

51. Clean up the sample with acetone, IPA, and DI water and dehydrate at 110 ℃ for 10 min.
52. Expose the micro-probes under UV ozone for 15 min.
53. Spin coat SU8-3005 epoxy onto the sample (500 rpm 9 s, 3000 rpm 30 s) and bake up the sample at 110 ℃ for around 10 s.
54. Transfer print the micro photodetector from the source GaAs wafer onto the sample with PDMS stamps.
55. Pattern SU8-3005 epoxy to expose contact pads of LED by UV lithography with a dose of 150 mJ/cm^2, and post-bake at 65 ℃ for 1 min and 95 ℃ for 3 min.
56. Develop in PGMEA for 2.5 min and rinse with IPA.
57. Hard bake at 110 ℃ for 30 min.

Micro-LED encapsulation

58. Clean up the sample with acetone, IPA, and DI water and dehydrate at 110 ℃ for 10 min.
59. Expose the micro-probes under UV ozone for 15 min.
60. Spin coat SU8-3005 epoxy onto the sample (500 rpm 9 s, 3000 rpm 30 s) and soft-bake at 65 ℃ for 1 min and 95 ℃ for 3 min.
61. Pattern SU8-3005 epoxy to expose contact pads of LED and electrodes on photodetector by UV lithography with a dose of 150 mJ/cm^2, and post-bake at 65 ℃ for 1 min and 95 ℃ for 3 min.
62. Develop in PGMEA for 2.5 min and rinse with IPA.
63. Hard bake at 110 ℃ for 30 min.

Micro photodetector metallization

64. Clean up the sample with acetone, IPA, and DI water and dehydrate at 110 ℃ for 10 min.
65. Spin coat AZ nLOF 2070 photoresist (500 rpm 9 s, 3000 rpm 30 s) and soft-bake at 110 ℃ for 2 min.
66. Pattern the conducting wires by UV lithography with a dose of 45 mJ/cm^2, and post-bake at 110 ℃ for 1 min.
67. Develop in an aqueous base developer (AZ300 MIF) for 1 min. Shake it at 50 seconds after the sample is placed in. Rinse with DI water.

68. Deposit 10 nm Cr / 600 nm Cu / 200 nm Au as the conducting wires.

69. Lift-off in acetone, and clean the sample with acetone, IPA and DI water.

Dye filter formation

70. Clean up the sample with acetone, IPA, and DI water and dehydrate at 110 ℃ for 10 min.

71. Expose the micro-probes under UV ozone for 15 min.

72. Spin coat mixture of ABS473 dye and SU8-3005 epoxy onto the sample (500 rpm 9 s, 3000 rpm 30 s) and soft-bake at 65 ℃ for 1 min and 95 ℃ for 3 min.

73. Pattern SU8-3005 epoxy to expose contact pads of LED and photodetector by UV lithography with a dose of 300 mJ/cm^2, and post-bake at 65 ℃ for 1 min and 95 ℃ for 3 min.

74. Develop in PGMEA for 2.5 min and rinse with IPA.

75. Hard bake at 110 ℃ for 30 min.

Encapsulation of the sample

76. Clean up the sample with acetone, IPA, and DI water and dehydrate at 110 ℃ for 10 min.

77. Expose the micro-probes under UV ozone for 15 min.

78. Spin coat SU8-3005 epoxy onto the sample (500 rpm 9 s, 3000 rpm 30 s) and soft-bake at 65 ℃ for 1 min and 95 ℃ for 3 min.

79. Pattern SU8-3005 epoxy to expose contact pads of LED and photodetector by UV lithography with a dose of 150 mJ/cm^2, and post-bake at 65 ℃ for 1 min and 95 ℃ for 3 min.
80. Develop in PGMEA for 2.5 min and rinse with IPA.
81. Hard bake at 110 ℃ for 30 min.

Laser milling

82. Use laser milling to cut the PI film into photometric probe shape (LPKF ProtoLaser U4, 365 nm; 1000 Hz, 0.5 W, 50 repeats + 1 W, 100 repeats + 2W, 40 repeats).

Device encapsulation

83. Expose the photometric probe under UV ozone for 15 min.
84. Dip coat the probe with PDMS.
85. Bake the probe in 75 ℃ for 2 h.
86. Coat the probe with a layer of parylene C (17 μm, Specialty Coating Systems).

Figure S1

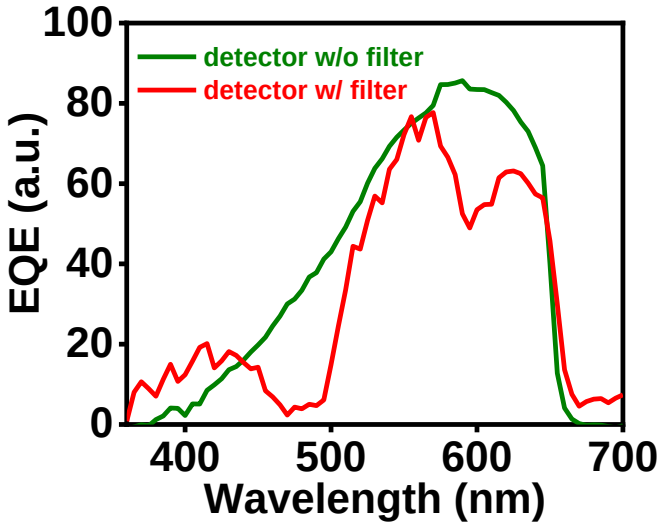

Figure S1. EQE of an InGaP detector with and without the dye filter coating.

Figure S2

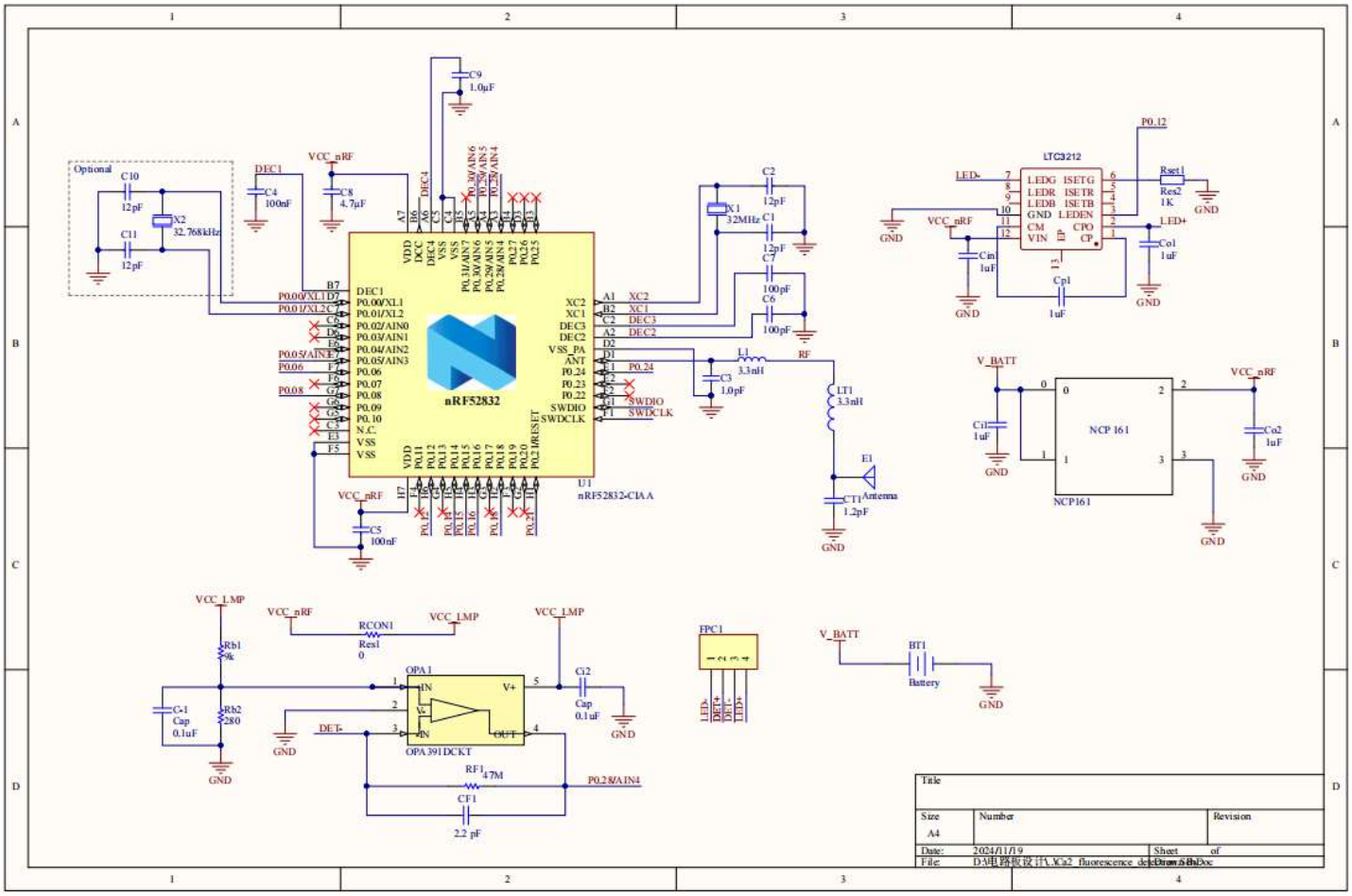

Figure S2. Schematic diagram of the wireless control module.

Figure S3

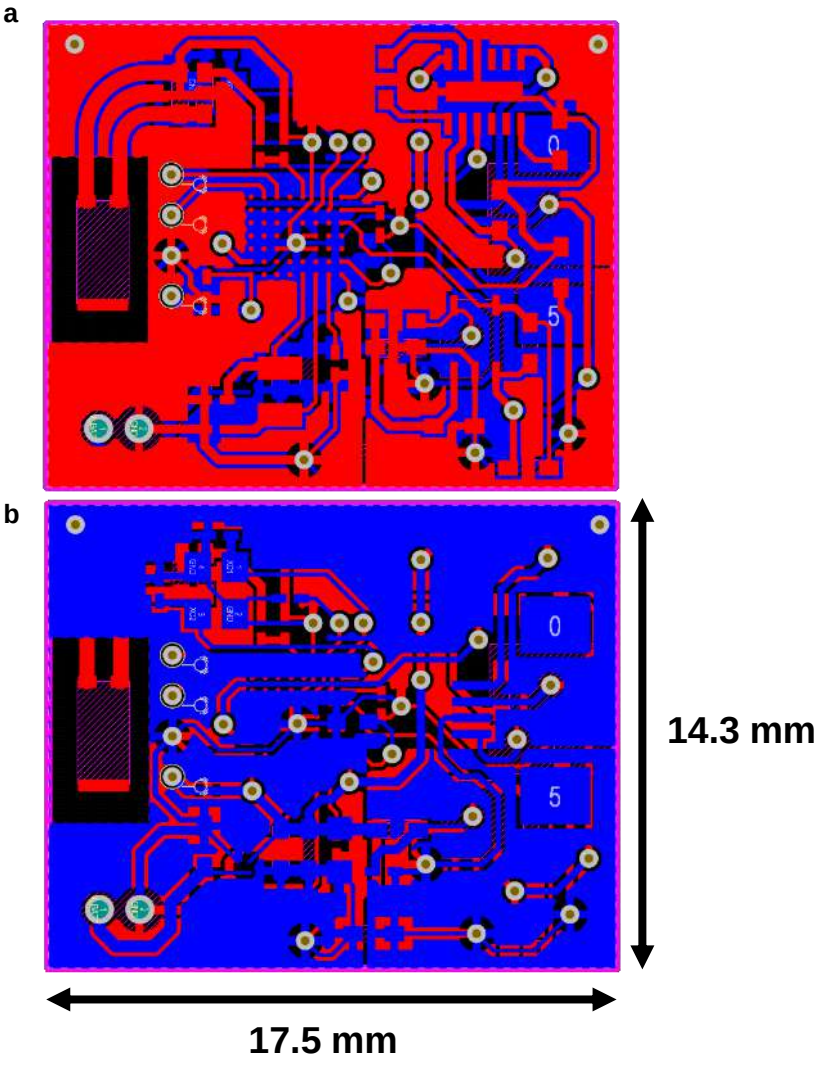

Figure S3. Layout of the designed printed circuit board. a) front view and b) back view.

Figure S4

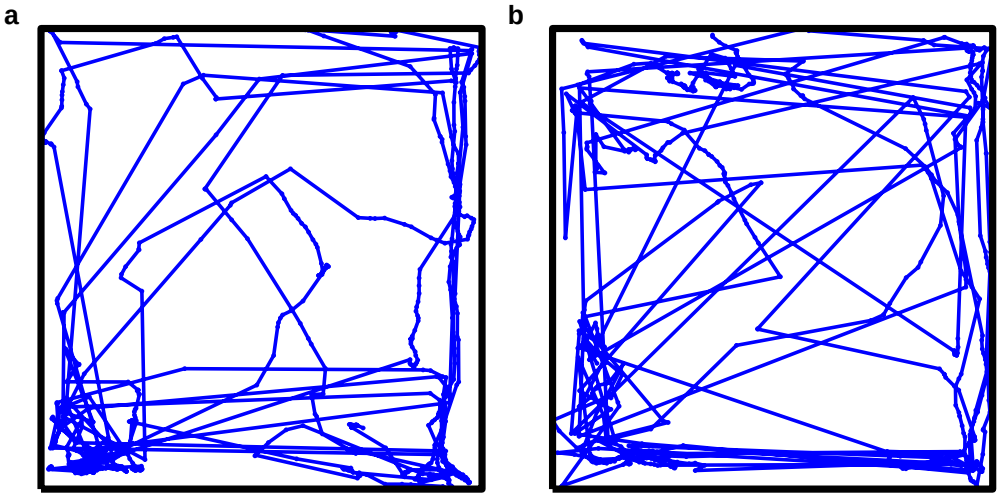

Figure S4. **Recorded trajectories for the freely moving mouse** a) with and b) without the wireless module in the test arena for 5 min (arena size: 40 cm × 40 cm).

Figure S5

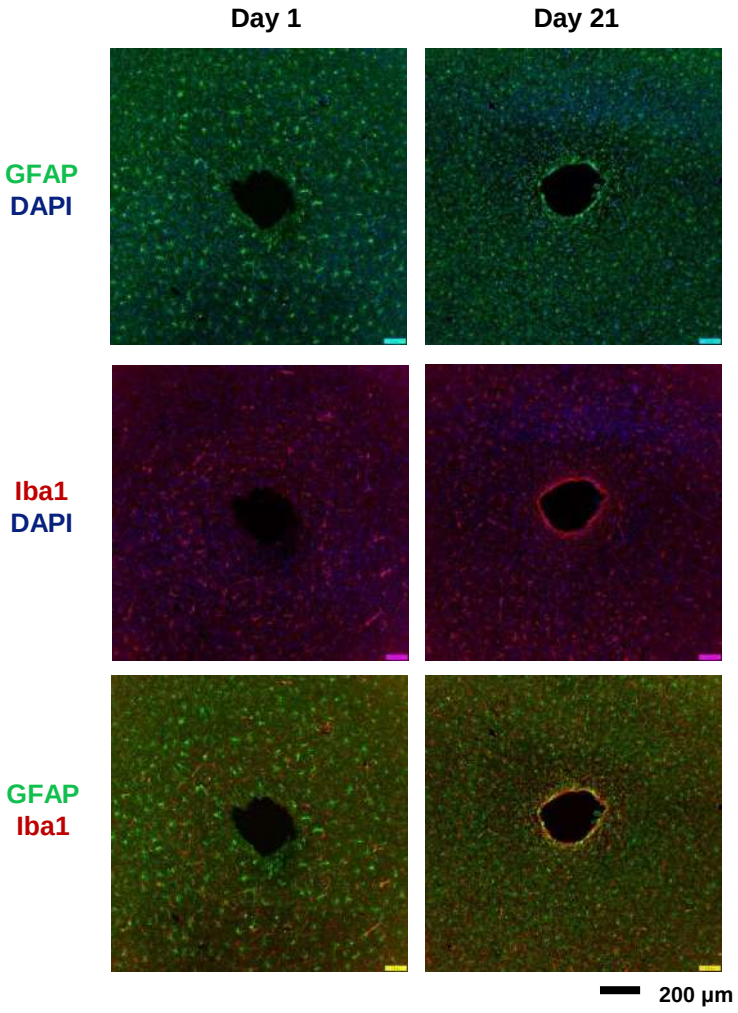

Figure S5. **Immunohistochemical staining** of astrocytes (GFAP) and activated microglia (Iba1) for brain slices with the probe after 1 day and 21 days implantation. Green: GFAP; Red: Iba1; Blue: DAPI.

Figure S6

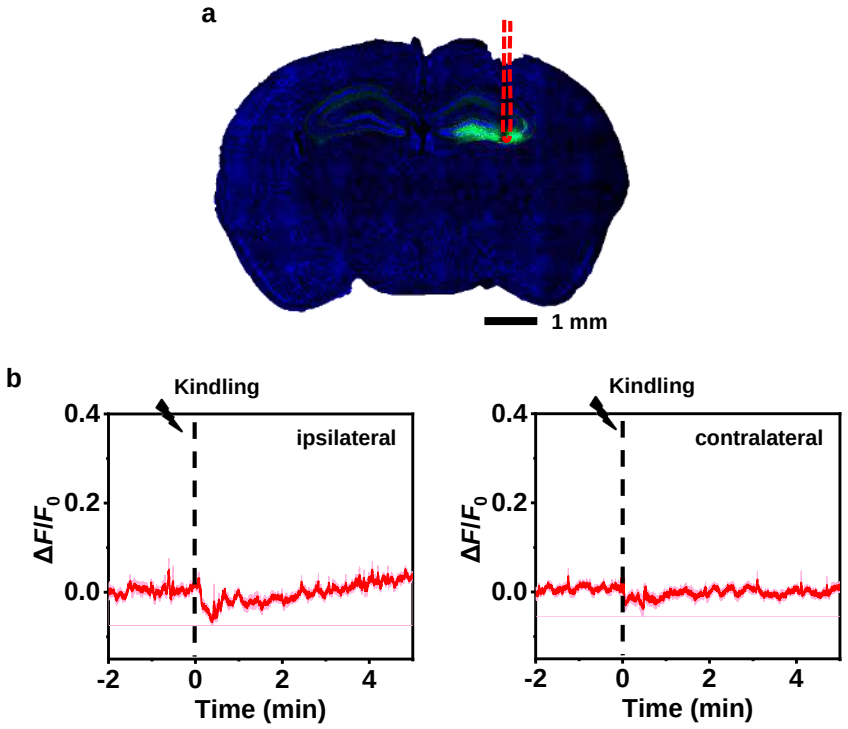

Figure S6. ***In vivo*** **Ca^{2+} fluorescence recording in the hippocampus (CA3) of mice with EGFP expression under electrical stimulation.** a) Fluorescence image showing immunohistochemical staining of nuclei (DAPI, blue) and neurons expressing EGFP (green) after probe implantation for 6 days. Lesion areas are outlined by red dashed lines. b) Averaged Ca^{2+} fluorescence spikes responding to kindling in the CA1 recorded in the ipsilateral (left, from 10 individual trials in n = 1 mice) and the contralateral (right, from 10 individual trials in n = 2 mice) CA3. The solid lines and shaded areas indicate the mean and s.e.m., respectively.

Table S1

materials	thickness (nm)
ITO	230
p+ GaN	120
Electron blocking layer	20
MQWs	130
Strained layers	300
n+ GaN	3000
u GaN	3500
sapphire substrate	-

Table S1. Epitaxial structure of the InGaN blue LED wafer.

Table S2

materials	thickness (nm)	doping (cm^{-3})	dopant
n+ $(Al_{0.7}Ga_{0.3})_{0.5}In_{0.5}P$ filter	500	2e18	Si
n+ GaAs contact	10	>6e18	Si
n+ $In_{0.5}Al_{0.25}Ga_{0.25}P$ window	30	5e18	Si
n+ $In_{0.5}Ga_{0.5}P$ emitter	100	2e18	Si
p- $In_{0.5}Ga_{0.5}P$ base	1000	3e16	Zn
p+ $In_{0.5}Ga_{0.5}P$ BSF	100	2e18	Mg
p+ GaAs contact	100	>5e18	Mg
p+ $In_{0.5}Ga_{0.5}P$ support	1000	2e18	Mg
$Al_{0.95}Ga_{0.05}As$ sacrificial	500	-	-
GaAs substrate	-	-	-

Table S2. Epitaxial structure of the InGaP detector wafer.